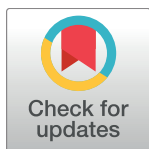# Predictive modelling of a novel anti-adhesion therapy to combat bacterial colonisation of burn wounds

Paul A. Roberts[1,2]*, **Ryan M. Huebinger[3]**, **Emma Keen[2]**, **Anne-Marie Krachler[4]**, **Sara Jabbari[1,2]**

1 School of Mathematics, University of Birmingham, Edgbaston, Birmingham, United Kingdom, **2** Institute of Microbiology and Infection, School of Biosciences, University of Birmingham, Edgbaston, Birmingham, United Kingdom, **3** Department of Surgery, University of Texas Southwestern Medical Center, Dallas, Texas, United States of America, **4** Department of Microbiology and Molecular Genetics, University of Texas McGovern Medical School at Houston, Houston, Texas, United States of America

* p.a.roberts@univ.oxon.org

Abstract

As the development of new classes of antibiotics slows, bacterial resistance to existing antibiotics is becoming an increasing problem. A potential solution is to develop treatment strategies with an alternative mode of action. We consider one such strategy: anti-adhesion therapy. Whereas antibiotics act directly upon bacteria, either killing them or inhibiting their growth, anti-adhesion therapy impedes the binding of bacteria to host cells. This prevents bacteria from deploying their arsenal of virulence mechanisms, while simultaneously rendering them more susceptible to natural and artificial clearance. In this paper, we consider a particular form of anti-adhesion therapy, involving biomimetic multivalent adhesion molecule 7 coupled polystyrene microbeads, which competitively inhibit the binding of bacteria to host cells. We develop a mathematical model, formulated as a system of ordinary differential equations, to describe inhibitor treatment of a *Pseudomonas aeruginosa* burn wound infection in the rat. Benchmarking our model against *in vivo* data from an ongoing experimental programme, we use the model to explain bacteria population dynamics and to predict the efficacy of a range of treatment strategies, with the aim of improving treatment outcome. The model consists of two physical compartments: the host cells and the exudate. It is found that, when effective in reducing the bacterial burden, inhibitor treatment operates both by preventing bacteria from binding to the host cells and by reducing the flux of daughter cells from the host cells into the exudate. Our model predicts that inhibitor treatment cannot eliminate the bacterial burden when used in isolation; however, when combined with regular or continuous debridement of the exudate, elimination is theoretically possible. Lastly, we present ways to improve therapeutic efficacy, as predicted by our mathematical model.

Author summary

Humankind is engaged in an arms race; one we are in danger of losing. Since the development and application of the first antibiotics, resistant strains of bacteria have steadily emerged. As the rate of discovery of new antibiotics slows, the threat increases. At present, 700,000 individuals globally die each year due to antimicrobial resistance and this number is predicted to rise to 10 million per year by 2050 unless fresh action is taken. It is important, therefore, that we explore alternative treatment strategies to replace or complement traditional antimicrobials. Here we use mathematical models to explain and predict the effects of a novel anti-adhesion therapy applied to infected burn wounds. This theoretically resistance-proof therapy operates by impeding bacteria from binding to host cells by blocking the host cell binding sites. This prevents bacteria from accessing nutrients and renders them susceptible to artificial clearance. Fitting our model to experimental data, we identify a number of valid parameter sets, and predict the conditions under which treatment will be effective for each set. These predictions are experimentally testable, and could be used to guide the development and application of anti-adhesion treatments in a clinical setting.

Introduction

As we begin to lose the arms race against microbial infections, it is important that we develop new treatment strategies as a complement or alternative to antibiotics. In this paper, we use mathematical modelling to explain and predict the effects of a novel anti-adhesion therapy in the treatment of infected burn wounds, with the aim of improving treatment outcome.

Each year, millions of lives are saved through the use of antibiotics to combat bacterial infections. However, sustained use of any given antibiotic leads to the clinical emergence of drug-resistant strains. Since the discovery of penicillin, many new classes of antibiotics have been identified, allowing clinicians to switch between antibiotics if resistance emerges either within an individual patient or within a patient population [1]. Over time, strains have emerged which exhibit resistance to multiple classes of antibiotics (multi-drug resistance) and reports of bacterial infections which are resistant to all known antibiotics (pan-resistant) are becoming increasingly common. At present, a reported 700,000 individuals worldwide die each year due to antimicrobial resistance and this figure is predicted to rise to 10 million per year by 2050 unless steps are taken to combat this threat [2]. While resistant strains continue to evolve, our ability to develop new classes of antibiotics is diminishing, the rate of antibiotic discovery having slowed significantly since its 'Golden Era' in the 1940s–1960s [1, 3]. It is therefore vital that we develop alternative treatment strategies to replace or complement antibiotics [4, 5].

One potential way forward is through the use of anti-virulence treatments. Whereas antibiotics either kill bacteria (bactericidal) or inhibit their growth (bacteriostatic), anti-virulence treatments interfere with a pathogen's ability to cause damage and disease in the host [6]. As such, they are likely to exert a smaller selective pressure upon a bacterial community, reducing the chances that resistance will develop (though opinions vary over the extent to which they may be resistance-proof, see [7, 8]). Anti-virulence treatments take a number of forms including those which target or inhibit toxin activity, adhesion, toxin secretion, virulence gene expression and inter-bacterial signalling [9–11].

In this paper, we consider a form of anti-adhesion treatment consisting of polystyrene microbeads coupled to a protein known as multivalent adhesion molecule (MAM) 7 (see also

[12] and other papers from their group for alternative anti-adhesion treatments that operate by blocking pilus assembly or function). MAM7 is anchored in the outer membrane of many Gram-negative bacteria, where it is responsible for initiating attachment of bacteria to host cells [13, 14]. When applied to an infection site, MAM7-coated beads (henceforth, inhibitors) act as a bacteriomimetic, competitively inhibiting the infectious agent from binding to host cells. This prevents bacteria from deploying those virulence mechanisms for which cell-to-cell contact is required and renders them more susceptible to natural or artificial physical clearance. Given that inhibitors must bind to host cells before bacteria in order to block them from binding, it is unclear whether their application may ever be expanded from prevention (prophylaxis) to the treatment of established infections (therapy).

Bacterial infection is a major cause of mortality in patients with burn wounds, where it is responsible for up to 75% of deaths in cases where severe burns are sustained to more than 40% of the body surface area [15]. Burn wounds are commonly infected by *Pseudomonas aeruginosa* [15–18], an opportunistic Gram-negative bacterium; the infection often being hospital-acquired (nosocomial) [15, 19].

Current treatment of such infections involves use of topical and systemic antibiotics, and regular debridement (mechanical wound cleaning). Debridement is either achieved through regular wound cleansing with a cloth, or through application of negative pressure devices (negative pressure wound therapy, NPWT) in which fluid is drawn out of the wound, either continuously or intermittently, using a pump, attached to a foam dressing covering the wound [20]. Some studies have shown NPWT to be effective in reducing the bacterial burden [21]; however, this result is not consistent across all studies [20, 22].

In earlier work we have shown, using an experimental model for *P. aeruginosa* burn wound infections in the rat, that treatment with inhibitors can significantly reduce the bacterial burden in the wound without impeding wound closure [23] (see Experimental set-up for more details). *In vitro* studies have also demonstrated the efficacy of inhibitor treatment in reducing cytotoxicity [9, 24] and have shown that inhibitors do not interfere with host cell functions critical to wound healing [25].

A number of mathematical modelling studies have considered the use of anti-virulence treatments to combat bacterial infections. The majority of these studies focus upon anti-quorum sensing treatments (see, for example, [26–33]). An exception to this rule; the model in [34] is of particular relevance to the present work. This ordinary differential equation (ODE) model considers a general anti-virulence treatment, which operates by enhancing innate immunity in bacterial clearance. The model predicts that, when used in isolation, anti-virulence treatment is unlikely to eliminate a bacterial infection. However, the model predicts that, when combined with antibiotics, anti-virulence treatments could eliminate bacteria, provided antibiotic and anti-virulence treatments are applied in staggered doses. Other modelling work has considered the bacterial invasion of burn wounds and the resultant tissue damage [30, 35–37], the influence of bacterial infection upon the healing of burn wounds [38] and the effects of ambient gas plasma treatment in this context [39]. Each of these models is formulated as a system of partial differential equations in one or two spatial dimensions. Models have also been developed to describe microbial adhesion to surfaces, for example, [40] developed an ODE model for the competitive colonisation of the gut wall by host and invader strains of *Escherichia coli*. Lastly, [41] have developed an individual-based model to describe the colonisation of a generic surface by phenotypically heterogeneous bacteria, in which bacteria may migrate between the surface and a liquid medium.

In this paper, we construct a mathematical model, formulated as a system of ODEs, to describe the population dynamics and treatment of a bacterial infection within a burn wound. Basing our mathematical model upon Huebinger *et al.*'s [23] experiments, we use it to explain

the empirical results and to predict the effects of various treatment regimes, involving inhibitor dosing and debridement, with the aim of improving efficacy. A particular strength of this study is that we consider multiple parameter sets, twelve in total, each of which provides a good fit to the experimental data. Classifying these sets into four qualitatively different cases, we consider the long-term effects of each treatment strategy, predicting the conditions under which treatment will eliminate the bacterial burden across all four cases.

Materials and methods

Experimental set-up

In this section we provide a simple description of the experimental set-up which forms the basis for our mathematical model. The experimental work was published previously in [23], wherein a more detailed description can be found.

We consider a burn wound infection model in the Sprague-Dawley rat (see Fig 1). Rats were anaesthetised and the portion of each rat which was to be burned was shaved. Rats were then immersed in 100˚C water for 12s resulting in full-thickness cutaneous burns to 40% of the body surface area, in a region spanning the back and upper sides of the body. We label the time at which the burn is administered as day −2. Rats were then resuscitated and given the appropriate pain control for the remainder of the experiment. On day 0, two days after the
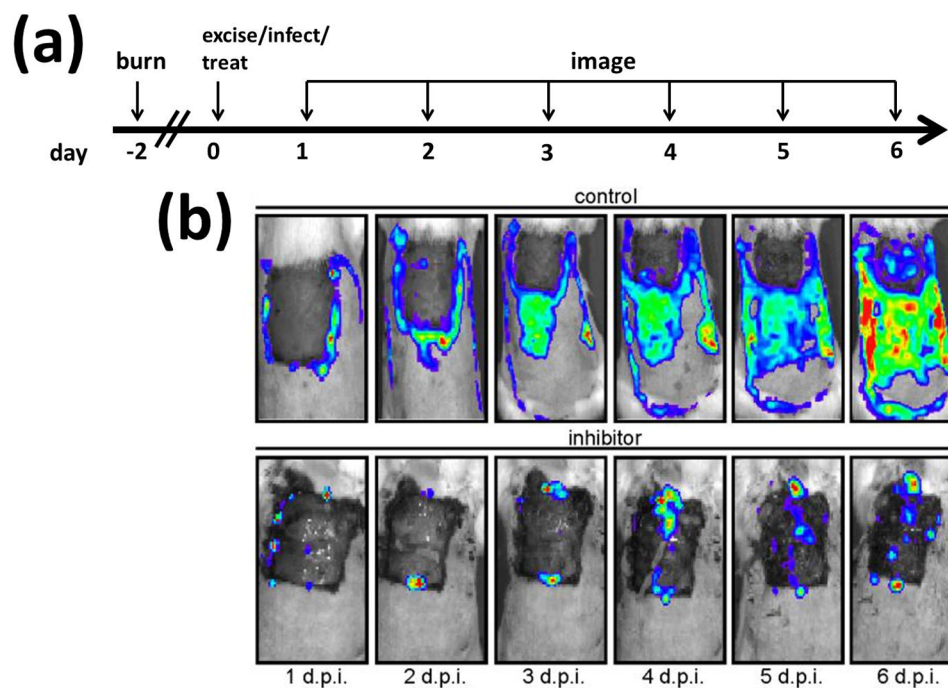
Fig 1. Diagram summarising the experimental set-up. (a) Burns were administered to the backs of the rats on day −2. On day 0 a region of eschar (dead) tissue was excised and bioluminescent *P. aeruginosa* were applied to the excision, followed by suspensions containing either inhibitor or control beads. Rats were imaged every 24 hours on days 1-6 post infection. (b) Exemplar images of burn wounds to which control beads (top) and inhibitor (bottom) were applied. In each image, the dark-grey area is the excision, the light-grey region is the non-excised burn wound, the white region is healthy, fur-covered tissue, and the coloured regions (colour online) denote the presence of bacteria, red corresponding to high density and blue to low density. The bacterial population increases in size and spreads much more rapidly across the burn wound in the control scenario than when inhibitor is used. See Experimental set-up for more details. d.p.i.: days post infection. Figure reproduced, with modifications, from [23], where it was published under a CC-BY 4.0 license.

https://doi.org/10.1371/journal.pcbi.1006071.g001

burn was administered, a section of eschar (dead) tissue, approximately 4×4 cm in area, was surgically excised. Next, 5×10^6 CFU (colony-forming units) of multidrug-resistant *P. aeruginosa* were applied to the excised region, followed by suspensions containing either 3×10^8 inhibitor or control beads (without a MAM7 coating) in saline. Identical inhibitor and control treatments were repeated every 24 hours for days 1–5 post infection; however, since a scab (i.e. a layer of solidified exudate) forms over the excision by day 1, treatments administered on or after day 1 are unlikely to enter the (liquid) exudate. Rats were euthanized after the experiment, on day 6.

A bioluminescent, multidrug-resistant *P. aeruginosa* isolate, Xen5, was chosen, such that the bacterial burden and their spatial distribution across the wound could be detected. An IVIS Spectrum *in vivo* imaging system (Perkin Elmer) was used to record bacterial luminescence on days 1–6 post infection, from which the total flux (photons sec^{-1}) was calculated using MetaMorph software (Molecular Devices) to integrate over the pixels. The total number of bacteria in CFU was then calculated using the conversion factor 4×10^8 photons sec$^{-1} \leftrightarrow 5 \times 10^6$ CFU, which was determined by measuring the luminescence of suspensions which contained an experimentally determined number of bacterial colony-forming units.

13 experiments were conducted using inhibitor and 11 using control beads. Two of the control bead experiments were discounted because the exposure setting used was too high to prevent the image from saturating. This may imply that the mean bacteria population size over time calculated for the control bead scenario slightly underestimates the true mean value. The experimental results are summarised in Fig 2.

These results raise two important questions:

1. *Why does treatment with inhibitor affect the bacterial population dynamics in this way?*

2. *How might the treatment be adapted to improve its efficacy?* For instance, this might be achieved by altering the adhesive properties of the inhibitor, the inhibitor dosing regimen or by combining inhibitors with other treatment strategies.

In what follows, we formulate a mathematical model of the burn wound infection experiment described above to help us answer these questions.

Model formulation

The burn wound is assumed to consist of two physical compartments: the host cells, and a fluid compartment exuded by the host cells and (hence) known as the *exudate*. The host cells and the overlying exudate extend to the perimeter of the burn wound beneath the necrotic tissue, while the exudate is exposed to the air at the excision (see Fig 3A). The area of the burn wound, A_r (cm^2), remains essentially fixed during the experiment; however, the exudate height, h (cm), and volume, V (cm^3), are elevated for a short period following the application of bacteria and inhibitors to the excision at the beginning of day 0 (see Fig 1A). This excess fluid is lost rapidly via run-off (down the sides of the rat), evaporation and absorption (into the host cells). Since the timescale over which the height and volume are elevated (on the order of minutes) is small compared to the timescale of the experiment (on the order of days), we neglect this variation and assume a fixed height and volume throughout the course of the experiment.

Both bacteria and inhibitors can exist in one of two states; either free in the exudate or bound to the host cells (we note that inhibitors do not bind to bacteria). It is assumed that the system is well-mixed since any given bacteria (or inhibitor) has an equal chance of interacting with any given binding site and since all other processes (growth, clearance, phagocytosis and unbinding) are thought not to depend upon their spatial location. This allows us to forgo an
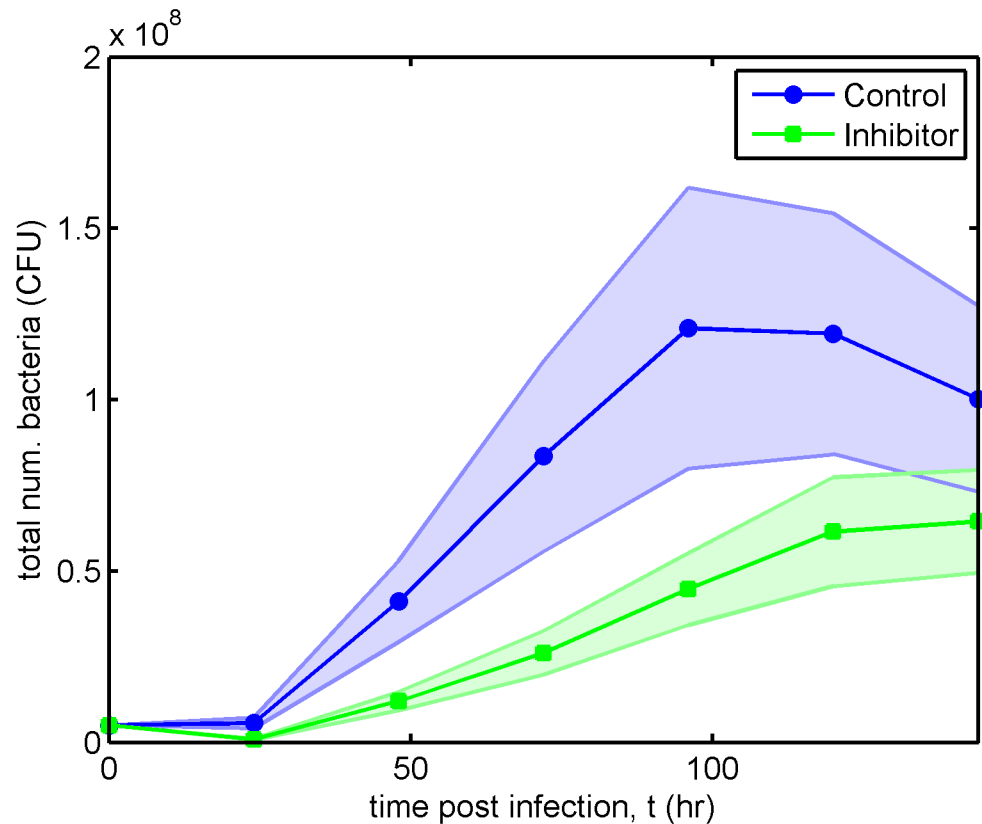
Fig 2. Bacterial population size for control bead and inhibitor treated rats in the experimental model. The discs and squares show the mean bacterial population size in control bead ($n = 9$ animals) and inhibitor ($n = 13$ animals) treated rats respectively, while the shaded regions show the standard error of the mean (that is, $\mu \pm \sigma/\sqrt{n}$, where μ is the mean and σ is the standard deviation). Treatment with the inhibitor reduces, but does not eliminate, the bacterial burden. CFU: colony-forming units.

https://doi.org/10.1371/journal.pcbi.1006071.g002

explicit spatial component and so to construct an ODE model for the evolution of the free bacteria density, $B_F(t)$ (cells cm^{-3}), bound bacteria density, $B_B(t)$ (cells cm^{-2}), free inhibitor concentration, $A_F(t)$ (inhibitors cm^{-3}), and bound inhibitor concentration, $A_B(t)$ (inhibitors cm^{-2}), over time, t (hr). It is assumed that the total binding site density on the host cells, consisting of both free and occupied sites, is conserved, such that the free binding site density $E(t) = E_{init} - \phi_{Bac}B_B(t) - \phi_A A_B(t)$ (sites cm^{-2}), where E_{init} (sites cm^{-2}) is the initial density of free binding sites, and ϕ_{Bac} (sites cell^{-1}) and ϕ_A (sites inhibitor^{-1}) are the number of binding sites occupied by a bacterium or an inhibitor respectively.

The model is summarised in Fig 3B and described by the following governing equations

$$
\frac{dB_F}{dt} = \underbrace{r_F B_F\left(1 - \frac{B_F}{K_F}\right)}_{\text{logistic growth}} + \underbrace{(1 - \eta(E))H(K_B - B_B)\frac{r_B}{h}B_B\left(1 - \frac{B_B}{K_B}\right)}_{\text{daughter cells freed from host cells upon division}} - \underbrace{\alpha_{Bac}A_r B_F E}_{\text{binding to host cells}}
$$

$$
+ \underbrace{\frac{\beta_{Bac}}{h}B_B}_{\substack{\text{unbinding} \\ \text{from host cells}}} - \underbrace{\psi_{Bac}(t)B_F}_{\text{natural clearance}},
$$

(1)
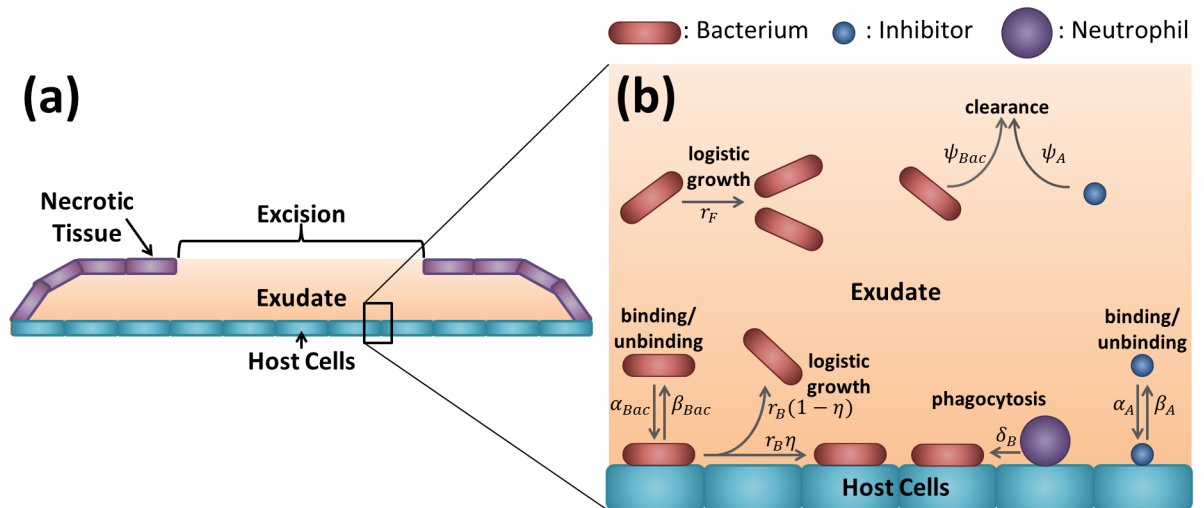
Fig 3. Diagrams showing the wound geometry and model structure. (a) Wound geometry pictured in the transverse plane. The host cells are covered by a liquid layer known as the exudate, which is itself covered by necrotic tissue, except in the region of the excision where the exudate is exposed to the air. (b) Diagram displaying the structure of the model given by Eqs 1–8. Bacteria and inhibitors exist in one of two states: free in the exudate or bound to the host cells, and can transition between these states by binding to (α_{Bac} and α_A) and unbinding from (β_{Bac} and β_A) the surface. Both free and bound bacteria can divide (r_F and r_B); daughters of free bacteria enter the exudate, whereas a proportion, $0 \leq \eta \leq 1$, of bound bacterial daughters remain bound to the surface, the remaining fraction, $1 - \eta$, entering the exudate. Bound bacteria may be phagocytosed by neutrophils (δ_B), while free bacteria and inhibitors are cleared from the wound in the first 24 hr after the excision is made and before a scab forms over the exposed exudate (ψ_{Bac} and ψ_A).

https://doi.org/10.1371/journal.pcbi.1006071.g003

$$\frac{\mathrm{d}B_B}{\mathrm{d}t} = \underbrace{(1 + (\eta(E) - 1)H(K_B - B_B))r_B B_B \left(1 - \frac{B_B}{K_B}\right)}_{\text{logistic growth (a proportion, } \eta, \text{ remain attached)}} + \underbrace{\alpha_{Bac} V B_F E}_{\substack{\text{binding to host cells}}} - \underbrace{\beta_{Bac} B_B}_{\substack{\text{unbinding} \\ \text{from host cells}}}$$

$$- \underbrace{\delta_B B_B}_{\text{phagocytosis}},$$
(2)

$$\frac{\mathrm{d}A_F}{\mathrm{d}t} = -\underbrace{\alpha_A A_r A_F E}_{\substack{\text{binding to} \\ \text{host cells}}} + \underbrace{\frac{\beta_A}{h} A_B}_{\substack{\text{unbinding} \\ \text{from host cells}}} - \underbrace{\psi_A(t) A_F}_{\substack{\text{natural} \\ \text{clearance}}},$$
(3)

$$\frac{\mathrm{d}A_B}{\mathrm{d}t} = \underbrace{\alpha_A V A_F E}_{\substack{\text{binding to} \\ \text{host cells}}} - \underbrace{\beta_A A_B}_{\substack{\text{unbinding} \\ \text{from host cells}}},$$
(4)

where parameter values are given in Tables 1 and 2, and Table A in S2 Supporting Information. See Parameter fitting and S1 Supporting Information for details on how the parameters were obtained. Note that we consider multiple parameter sets, each of which provides a good fit to the data.

Both free and bound bacteria are assumed to grow logistically with respective intrinsic growth rates r_F (hr^{-1}) and r_B (hr^{-1}), and carrying capacities K_F (cells cm^{-3}) and K_B (cells cm^{-2}). We interpret the carrying capacities to represent the maximum number of bacteria that can be sustained by available nutrients and the situation in which $B_F(t) = K_F$, or $B_B(t) = K_B$, to be one

Table 1. Fitted parameter values for Eqs 1–8.

Parameter	Description (Units)	Value			
		Case A	Case B	Case C	Case D
r_F	Intrinsic growth rate of free bacteria (hr^{-1})	8.37×10^{-2}	2.10×10^{-3}	4.18×10^{-3}	2.57×10^{-1}
r_B	Intrinsic growth rate of bound bacteria (hr^{-1})	1.10×10^{-1}	1.35×10^{-1}	1.50×10^{-1}	5.55
K_F	Carrying capacity of free bacteria (cells cm^{-3})	1.17×10^{7}	1.15×10^{6}	3.12×10^{6}	1.85×10^{6}
K_B	Carrying capacity of bound bacteria (cells cm^{-2})	9.96×10^{5}	1.65×10^{6}	1.48×10^{6}	1.43×10^{6}
α_{Bac}	Binding rate of bacteria to host cells (hr^{-1} sites^{-1})	1.34×10^{-9}	3.09×10^{-10}	2.32×10^{-10}	3.34×10^{-11}
β_{Bac}	Unbinding rate of bacteria from host cells (hr^{-1})	1.97×10^{-1}	4.11×10^{-9}	8.23×10^{-9}	5.79×10^{-6}
δ_B	Rate of phagocytosis of bacteria by neutrophils (hr^{-1})	1.06×10^{-3}	2.31×10^{-4}	3.97×10^{-4}	3.02×10^{-5}
η_{max}	Maximum proportion of daughters of bound cells that can enter the bound compartment (dimensionless)	2.95×10^{-2}	1.31×10^{-7}	3.06×10^{-7}	1.52×10^{-2}
γ	Concentration of binding sites at which $\eta = \eta_{max}/2$ (sites cm^{-2})	3.12×10^{4}	1.83×10^{5}	3.66×10^{4}	1.65×10^{6}
$\tilde{\psi}_{Bac}$	Natural clearance rate of bacteria (hr^{-1})	1.42×10^{-1}	2.13×10^{-6}	7.68×10^{-6}	5.01×10^{-1}
α_A	Binding rate of inhibitors to host cells (hr^{-1} sites^{-1})	1.46×10^{-6}	1.56×10^{-10}	2.32×10^{-10}	5.51×10^{-9}
β_A	Unbinding rate of inhibitors from host cells (hr^{-1})	6.35×10^{-8}	4.11×10^{-9}	3.85×10^{-3}	4.43×10^{-1}
$\tilde{\psi}_A$	Natural clearance rate of inhibitors (hr^{-1})	4.39×10^{-8}	2.13×10^{-6}	3.85×10^{-3}	1.75×10^{-5}
α_{Bac}/β_{Bac}	Bacterial association constant (sites^{-1})	6.82×10^{-9}	7.53×10^{-2}	2.82×10^{-2}	5.77×10^{-6}
α_A/β_A	Inhibitor association constant (sites^{-1})	2.29×10^{1}	3.79×10^{-2}	6.03×10^{-8}	1.24×10^{-8}
$\frac{(\alpha_{Bac}/\beta_{Bac})}{(\alpha_A/\beta_A)}$	Ratio of association constants (dimensionless)	2.97×10^{-10}	1.98	4.68×10^{5}	4.65×10^{2}

The last three rows give the bacteria association constant, α_{Bac}/β_{Bac}, the inhibitor association constant, α_A/β_A, and the ratio of bacteria to inhibitor association constants. Values are given to an accuracy of 3 significant figures.

https://doi.org/10.1371/journal.pcbi.1006071.t001

in which the rate of bacterial division is negligible (see [42, 43]). The burn wound exudate contains glucose and other nutrients and has been shown to be capable of supporting a proliferating population of *P. aeruginosa* [44, 45]. We note that, in general, $K_B \neq E_{init}/\phi_{Bac}$, such that the number of bacteria that can be nourished on the host cells is not equal to the number that can bind to the host cells. For all of the parameter sets considered in this paper, $K_B < E_{init}/\phi_{Bac}$ (see Tables 1 and 2, and Table A in S2 Supporting Information).

It is assumed that bacteria and inhibitors bind to and unbind from the host cells in accordance with the law of mass action, with respective binding rates α_{Bac} (hr^{-1} sites^{-1}) and α_A (hr^{-1} sites^{-1}), and unbinding rates β_{Bac} (hr^{-1}) and β_A (hr^{-1}).

Table 2. Measured, calculated and estimated parameter values for Eqs 1–8.

Parameter	Description (Units)	Value	Source
ϕ_{Bac}	Number of binding sites occupied by a bacterium (sites cell^{-1})	1	Estimated
ϕ_A	Number of binding sites occupied by an inhibitor (sites inhibitor^{-1})	1	Calculated
V	Volume of the exudate (cm^3)	4.9 (4.6)	Calculated
A_r	Area of the burn wound (cm^2)	49 (46)	Measured
h	Height of the exudate (cm)	0.1	Measured
n	Hill coefficient (dimensionless)	1	Estimated
$B_{F_{init}}$	Initial density of free bacteria (cells cm^{-3})	1.02×10^{6} (1.09×10^{6})	Measured
$A_{F_{init}}$	Initial concentration of free inhibitors (inhibitors cm^{-3})	0 or 6.12×10^{7} (6.52×10^{7})	Measured
E_{init}	Initial density of binding sites (sites cm^{-2})	2.57×10^{6}	Calculated

Measured values are those which have been measured directly, calculated values are those which have been calculated using values which were measured directly and estimated values are those which could not be measured or calculated. The values in brackets are used only when fitting the inhibitor treatment data to the model.

https://doi.org/10.1371/journal.pcbi.1006071.t002

Examination of histological sections through the burn wound shows that neutrophils are present within and at the surface of the host cells, but not within the exudate [23]. Administration of a burn wound causes neutrophils to be fully activated such that no further neutrophils are recruited in response to the bacterial infection [23, 46] (in contrast to [34]). Therefore, the immune response can be captured by the exponential decay of bound bacteria with rate δ_B (hr^{-1}), where δ_B accounts for the density of neutrophils. It is assumed that inhibitor degradation, if it occurs, is sufficiently gradual that it can be neglected.

Several of the terms in Eqs 1–4 contain h, A_r or V as a factor in order to ensure dimensional consistency. These constants could have been combined with other parameters, but we retain them in the interests of clarity.

A proportion of the daughter cells of bound bacteria, $0 \leq \eta(E(t)) \leq 1$ (dimensionless), remain bound to the surface, while the remaining fraction, $1 - \eta(E(t))$, enter the exudate. Daughter cells may not bind immediately either because the long axis of the parent cell is angled away from the host cell surface upon division or due to a lack of free binding sites on the neighbouring host cell surface. The proportion that remains bound, $\eta(E(t))$, depends upon the density of free binding sites, $E(t)$, such that a larger fraction of the daughter cells remain bound when more binding sites are available. We capture this dependence using a Hill function with constant γ (sites cm^{-2}) and Hill coefficient n (dimensionless) as follows

$$\eta(E) = \frac{\eta_{max} E^n}{\gamma^n + E^n},\tag{5}$$

where η_{max} (dimensionless) is the maximum proportion of daughter cells which may remain bound to the surface. If the density of bound cells, $B_B(t)$, exceeds the bound carrying capacity, K_B, then the bound logistic growth term becomes a death term. In this case, the loss of bacteria is confined to the bound compartment and does not affect the free compartment. This is achieved through the use of a Heaviside step function, $H(K_B - B_B(t))$, in Eqs 1 and 2, where

$$H(x) := \begin{cases} 0 & \text{if } x < 0, \\ 1 & \text{if } x \geq 0. \end{cases} \tag{6}$$

The rates of clearance of bacteria and inhibitors, $\psi_{Bac}(t)$ (hr^{-1}) and $\psi_A(t)$ (hr^{-1}), vary with time, such that clearance occurs at a constant rate for the first 24 hours and then stops after this point due to the formation of a scab over the excision. Thus, clearance occurs at rates

$$\psi_{Bac}(t) = \tilde{\psi}_{Bac} H(24 - t) \qquad \text{and} \qquad \psi_A(t) = \tilde{\psi}_A H(24 - t),\tag{7}$$

where $\tilde{\psi}_{Bac}$ (hr^{-1}) and $\tilde{\psi}_A$ (hr^{-1}) are the constant rates of clearance in the first 24 hours, and H is a Heaviside step function, as defined in Eq 6.

We choose the time $t = 0$ (hr) to correspond to the point at which bacteria and inhibitors are applied to the burn wound following the excision. Bacteria and inhibitors are present only in the free compartment initially, not having had the opportunity to bind to the host cells, such that

$$B_F(0) = B_{F_{init}}, \qquad B_B(0) = 0, \qquad A_F(0) = A_{F_{init}}, \qquad A_B(0) = 0,\tag{8}$$

where $B_{F_{init}}$ and $A_{F_{init}}$ are constants. See Tables 1, 2 and Table A in S2 Supporting Information for parameter values.

The parameters in Table 1 and Table A in S2 Supporting Information were fitted to the experimental data (see Parameter fitting and S1 Supporting Information for details), while those in Table 2 were either measured, calculated or estimated. The area of each burn wound

was determined from images, such as those in Fig 1, using the MetaMorph software, while the height of the fluid layer was measured to be 1 mm. As described in Experimental set-up, the initial density of bacteria and the initial concentration of inhibitor are known. The volume of the exudate is calculated as the product of the wound area and the height of the exudate. We know that there are about 1.5×10^5 host cells per cm^2 and that approximately 17 inhibitors may bind per host cell [9]. Taking the product of these two values gives us the initial density of free binding sites, E_{init}. We define a binding site to consist of the number of host cell binding receptors occupied by an inhibitor, such that an inhibitor occupies a single site and hence $\phi_A = 1$ sites inhibitor^{-1}. Inhibitors have been designed to occupy the same number of host cell binding receptors as a bacterium. Therefore, we also have that $\phi_{Bac} = 1$ sites cell^{-1}. We note that while an inhibitor occupies the same number of binding sites as a bacterium, a rod-shaped *P. aeruginosa* cell (which we have measured to be approximately 1μm×3μm) covers up to three times the host cell surface area as a spherical (1 μm diameter [23]) inhibitor without occupying any more sites. Simulations were found to be insensitive to the value of the Hill coefficient, n; therefore, we set it to unity for simplicity.

We leave our equations in dimensional form so as to make them easier to interpret biologically and since non-dimensionalisation would not reduce the number of fitted parameters (although it does reduce the total number of parameters).

Treatment scenarios

In addition to the untreated/control ($A_{F_{init}} = 0$) and single inhibitor dose ($A_{F_{init}} > 0$) scenarios based upon Huebinger *et al.*'s [23] experiments (see Experimental set-up), we consider a further six theoretical scenarios, five of which include either regular or continuous debridement (see Table 3). Since inhibitors operate by blocking bacteria from binding to the wound host cells, it is intuitive that this may result in the majority of bacteria occupying the free compartment. Thus, any treatment, such as debridement, which removes the exudate, could clear the free compartment of bacteria—and with them, inhibitors—significantly reducing the total population size of bacteria when combined with an inhibitor treatment. (Bound bacteria and inhibitors are left mostly intact by debridement.)

Table 3. Treatment scenarios.

Treatment scenario	Description
No treatment	No inhibitors or debridement are applied
Single inhibitor dose	Inhibitors are applied at time t = 0 hr
Regular inhibitor doses	Inhibitors are applied at time t = 0 hr, then again at t = 48 hr and reapplied every 24 hr
Regular debridement	All free bacteria and inhibitors are removed at t = 48 hr and the procedure repeated every 24 hr
Single inhibitor dose with regular debridement	Inhibitors are applied at time t = 0 hr, after which all free bacteria and inhibitors are removed at t = 48 hr and the debridement event repeated every 24 hr
Regular inhibitor doses with regular debridement	Inhibitors are applied at time t = 0 hr, and free bacteria and inhibitors are removed at t = 48 hr directly after which inhibitors are reapplied, the debridement-inhibitor treatment is then repeated every 24 hr
Continuous debridement	All free bacteria and inhibitors are removed at t = 48 hr, after which clearance of bacteria and inhibitors is maintained at a high level
Single inhibitor dose with continuous debridement	Inhibitors are applied at time t = 0 hr, and all free bacteria and inhibitors are removed at t = 48 hr, after which clearance of bacteria and inhibitors is maintained at a high level

Regular debridement consists of a series of discrete instantaneous debridement events, while continuous debridement consists of a sustained, high level of clearance ($\psi_{Bac} = \psi_A = 1000 \text{ hr}^{-1}$) and may be thought of as the limiting case of regular debridement in which the time between debridement events tends to zero. While it may not be possible to maintain such a high rate of clearance in practice, this clearance rate is chosen to determine the theoretical best-case-scenario were such a treatment to be applied. Following a discrete debridement event, it is assumed that the fluid compartment is restored on the timescale of a few minutes, such that the volume fluctuation can be neglected.

For each of the treatment strategies, Eqs 1–8 were solved using the Matlab routine `ode15s`, a variable-step, variable-order solver based upon numerical differentiation formulas.

The untreated and single inhibitor dose scenarios are those considered in the experiments and are described above and in Experimental set-up. The key difference between the numerical simulations (see Numerical solutions) and the experiments is that the simulations extend beyond the time frame of the experiments.

In the regular inhibitor dose scenario (and the regular inhibitor dose with regular debridement scenario), the repeat doses of inhibitors are identical to the initial dose, $A_{F_{init}}$. The second dose is not applied until 48 hr for consistency with the treatments involving debridement (see below). As noted in Experimental set-up, a scab forms over the wound after the first 24 hr, ending clearance and preventing further inhibitor doses from reaching the exudate. Thus, in practice, inhibitor doses could not be repeated without removing the scab and incurring further clearance at levels similar to those in the first 24 hr. However, since we are interested in the theoretical effect of repeated inhibitor doses independent of clearance, we neglect further clearance effects in this case. Were we to include additional clearance upon re-treatment with inhibitor, treatment efficacy would be improved.

In the scenarios involving regular debridement, clearance is re-established for the first 24 hours after each debridement event, with rates given in Table 1 and Table A in S2 Supporting Information, to account for leakage due to the loss of the scab upon debridement. The first debridement event is chosen to occur at $t = 48$ hr, rather than some earlier time, so as to give the inhibitors time to bind to the host cells.

Sensitivity analyses

We present two sets of sensitivity analyses. The first set (presented in Case A–Case D) shows the effect of a tenfold increase or decrease in each of the 13 fitted parameters, r_F, r_B, K_F, K_B, α_{Bac}, β_{Bac}, δ_B, η_{max}, γ, $\tilde{\psi}_{Bac}$, α_A, β_A and $\tilde{\psi}_A$, on the total number of bacteria either at steady-state (treatment scenarios 1 and 2) or at $t = 90$ days $= 2160$ hr (treatment scenarios 3–8; Figs O–V in S2 Supporting Information). We truncate the simulations for the latter treatment scenarios at 90 days since simulating treatments with regular inhibitor doses or regular debridement is computationally expensive and those involving continuous debridement are close to steady-state by this time. We note that the total population size of bacteria oscillates in those treatments that involve regular debridement, undergoing a sharp drop upon each debridement event. We plot the value of $B_T(t)$ at the peak of the oscillation at $t = 90$ days (directly prior to debridement), since we consider that it is by the maximum number of bacteria that the efficacy of a treatment should be judged.

In the second set of sensitivity analyses (presented in Inhibitor sensitivity analysis), we consider the effect of varying the binding and unbinding rates of inhibitors, α_A and β_A, in the space $\{10^{-12}, 10^{-11}, \ldots, 1\} \times \{10^{-12}, 10^{-11}, \ldots, 1\}$ upon the total number of bacteria at 4 weeks ($= 672$ hr) post infection in the 5 scenarios that involve inhibitor treatment (Figs W, Y, AA, AC and AE in S2 Supporting Information). We also consider the effect of increasing all

inhibitor doses by 10 fold from 6.12×10^7 inhibitors cm^{-3} (the standard value) to 6.12×10^8 inhibitors cm^{-3} (Figs X, Z, AB, AD and AF in S2 Supporting Information).

Parameter fitting

A combination of Markov Chain Monte Carlo (MCMC) and frequentist methods were used to fit the model given by Eqs 1–8 to the mean of the experimental data in the untreated and single inhibitor dose scenarios. Unfortunately, we have insufficient data to generate informative posterior distributions using the MCMC method; however, we are able to identify a number of good fits (twelve parameters sets are presented here) and to classify these into four general cases—A, B, C and D—based upon their qualitative behaviour (see Results). By considering a range of valid parameter sets, rather than a single good fit, we are able to gain a more comprehensive understanding of the model behaviour. The fitting procedures used differ between parameter sets and are summarised in Table A in S1 Supporting Information. See S1 Supporting Information for more details. We confirmed these fits with a nonlinear mixed-effects model using the Matlab routine `sbiofitmixed`, with parameter sets 1–12 as initial guesses.

Model fits are compared against the experimental data in Fig 4 and Figs A and B in S2 Supporting Information, where parameter sets 2 (Case A), 3 (Case B), 8 (Case C) and 12 (Case D) are presented in Fig 4. Since the experimental data does not distinguish between free and bound bacteria, we compare it against the simulated total number of bacteria, $B_T(t) = VB_F(t) + A_rB_B(t)$. The model achieves a good fit to the experimental mean in all cases, remaining mostly within the shaded region denoting the standard error of the mean.

Results

In what follows, we examine the behaviour of Eqs 1–8 in each of the four cases, A–D. For clarity, the results from four representative parameter sets, one from each case, are presented in the main text: Set 2 from Case A, Set 3 from Case B, Set 8 from Case C and Set 12 from Case D. For the complete set of results, see S2 Supporting Information. We begin with a steady-state analysis of the system with and without a single inhibitor dose in order to determine the number of steady-states and their stability properties. We then consider the behaviour of the time-dependent problem, simulating the bacterial population dynamics well beyond the time frame of the experiments. While simulations provide a good fit to the experimental data for all parameter sets, the model predictions diverge for later times. We investigate why a single inhibitor dose is or is not effective in each case in the long-term and explore other potential treatment strategies with the aim of improving efficacy. We consider a treatment to be effective if it reduces the bacterial burden and to be fully effective if the bacterial burden is eliminated (such that $B_T(t) < 1$).

Steady-state analysis

Steady-state analyses of Eqs 1–6, in the absence of clearance, with and without a single dose of inhibitors were performed using Maple. Clearance was neglected since leakage of fluid from the wound only occurs in the first 24 hours. It was found that the system has two physically realistic steady-states in both the untreated and single inhibitor dose scenarios for all 12 parameter sets. In each case the first steady-state, at which bacteria are absent, is unstable, while the second steady-state, at which both free and bound bacteria are present, is stable (see S3 Supporting Information for more details). By characterising the stability of the system in this way, we can be sure that we are not overlooking any potential stable steady-state solutions in the time-dependent simulations below.
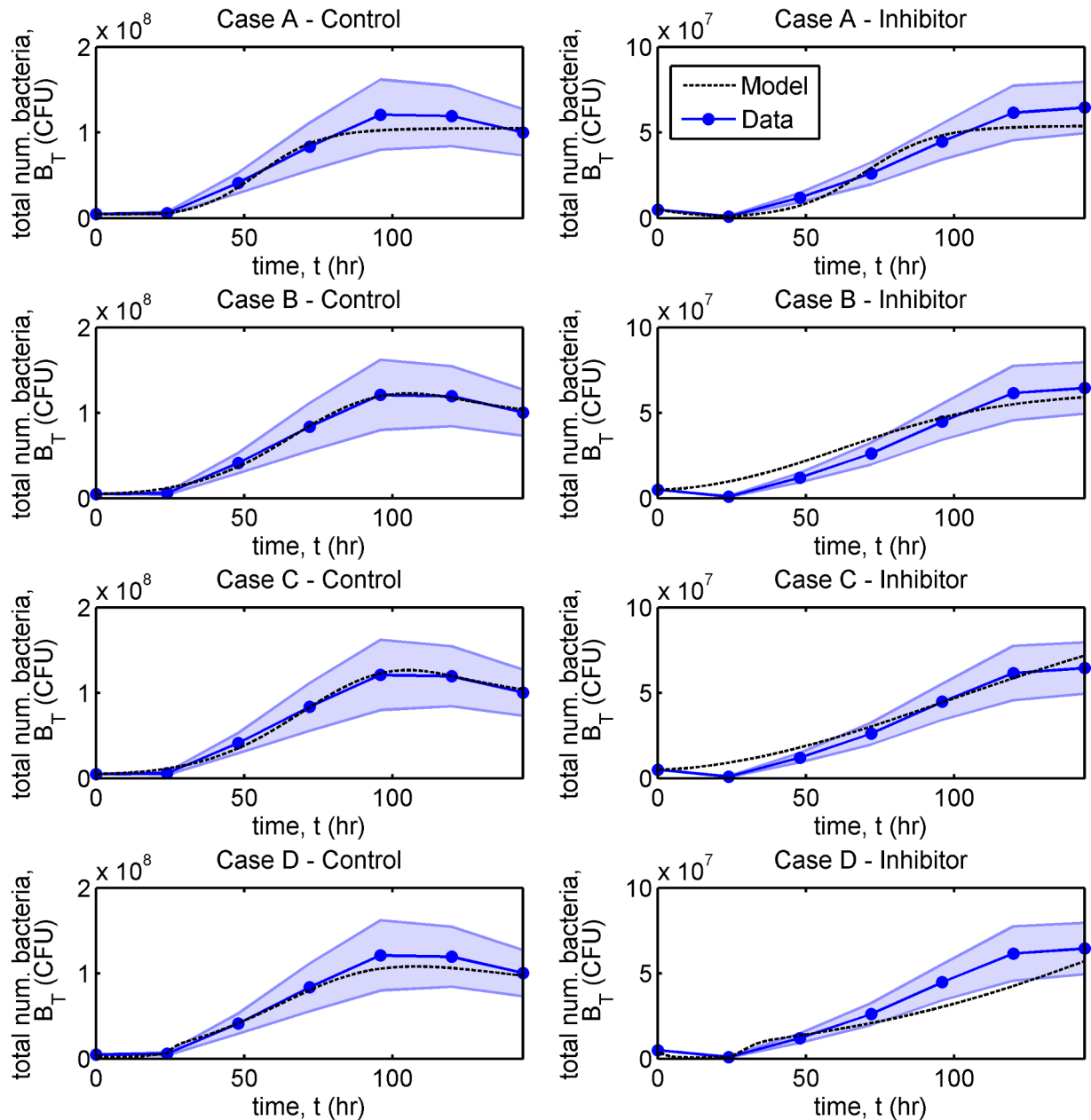
Fig 4. Comparison of model predictions with experimental data. The discs mark the experimental mean, while the shaded region shows the standard error of the mean. Simulation results, denoted by the dashed line, show the total number of bacteria, $B_T(t)$ $(= VB_F(t) + A_r B_B(t))$. Note that the range of the y-axis for the untreated (control) scenario (left-hand column) is twice that for the single inhibitor dose scenario (right-hand column). There is good agreement between the model and the data in all cases and the overall goodness of fit (mean squared error) is similar for each parameter set. Eqs 1–8 were solved using `ode15s` and fitting was performed using a combination of MCMC and frequentist methods (see Parameter fitting and S1 Supporting Information). See Tables 1 and 2 for parameter values. CFU: colony-forming units.

https://doi.org/10.1371/journal.pcbi.1006071.g004

Numerical solutions

Having explored the behaviour of the system at steady-state, we consider the full time-dependent problem (Eqs 1–8). We begin by making a few general comments, before taking Cases A–D in turn. Further details can be found in S4 Supporting Information.
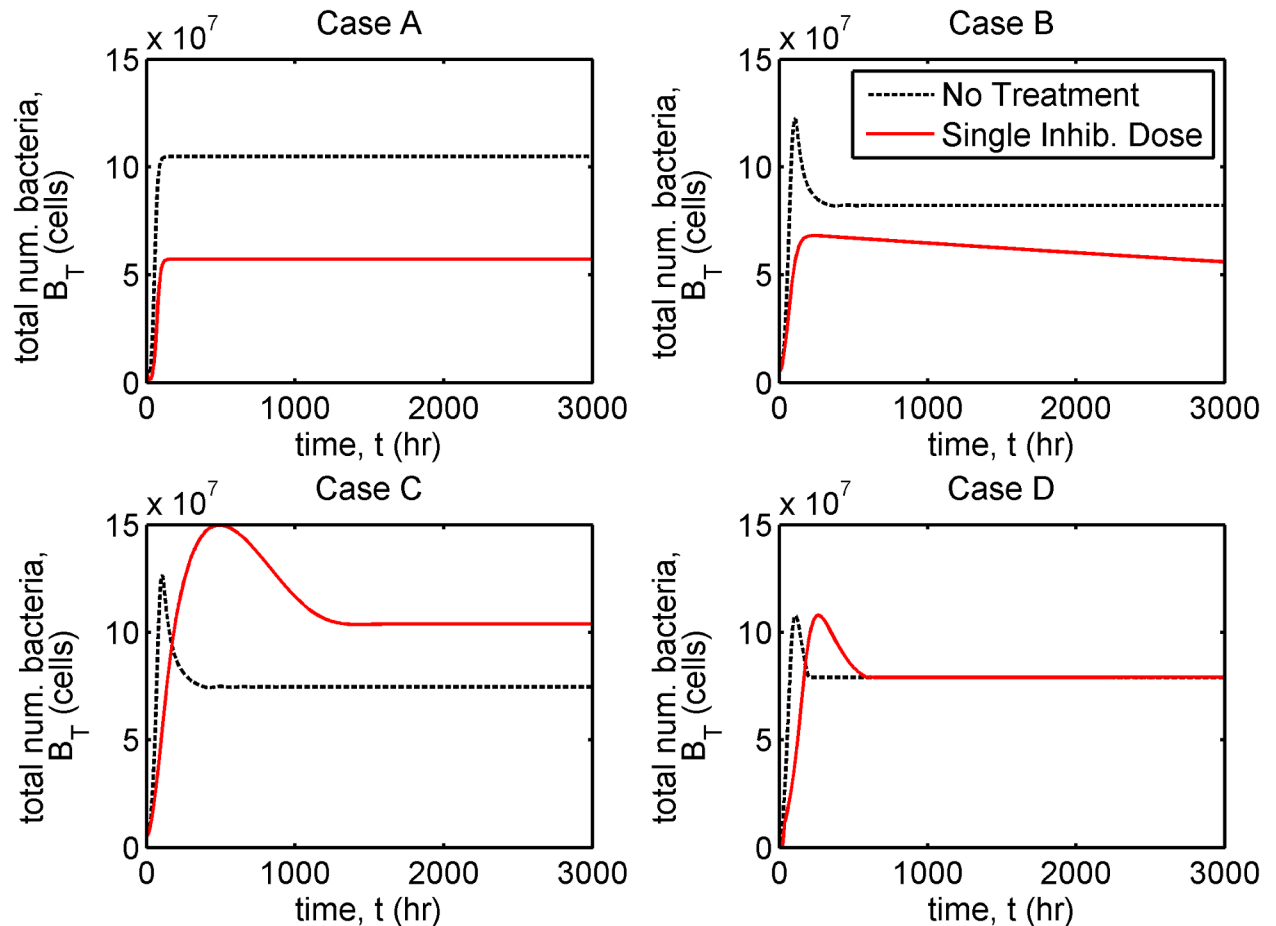
Fig 5. Comparison of bacterial population dynamics in the untreated and single inhibitor dose scenarios. The total number of bacteria, $B_T(t)$ ($= VB_F(t) + A_rB_B(t)$), is plotted in each case. Simulations extend beyond the time span of the experiments, to 3000 hours = 125 days. Case A: the bacterial population size is an essentially monotone increasing function of time in both untreated and treated scenarios, reaching an early steady-state at which the bacterial population size with treatment is roughly half that without; Case B: the bacterial population size with treatment remains below that without treatment, decreasing gradually after reaching an early maximum; Case C: treatment results in a sustained and significant increase in the bacterial population size, Case D: treatment causes the bacterial population size to temporarily exceed that without treatment, settling to a steady-state close to that of the untreated scenario. Eqs 1–8 were solved using `ode15s`. See Tables 1 and 2 for parameter values.

https://doi.org/10.1371/journal.pcbi.1006071.g005

In each case we present results to show the evolution in the total number of bacteria, $B_T(t) = VB_F(t) + A_rB_B(t)$ (Fig 5, and Fig D in S2 Supporting Information), the total numbers of free and bound bacteria, $\hat{B}_F(t) = VB_F(t)$ and $\hat{B}_B(t) = A_rB_B(t)$, free and bound inhibitors, $\hat{A}_F(t) = VA_F(t)$ and $\hat{A}_B(t) = A_rA_B(t)$, and free binding sites, $\hat{E}(t) = A_rE(t)$ (Fig 6, and Figs E and F in S2 Supporting Information), and of the individual terms in Eqs 1–4 (Figs G–L in S2 Supporting Information) in the untreated and single inhibitor dose scenarios. We also present results to show the evolution in the total number of bacteria in the treatment scenarios involving regular inhibitor doses and regular or continuous debridement (Fig 7, and Figs M and N in S2 Supporting Information). Lastly, we present a sensitivity analysis showing the effects of a tenfold increase or decrease in each of the 13 fitted parameters (Figs O–V in S2 Supporting Information, see Sensitivity analyses for details).

In the remainder of this paper, we distinguish between rate constants, e.g., α_{Bac} and δ_B, and the rate at which processes occur, e.g., $\alpha_{Bac}A_rB_FE$ and δ_BB_B, the former being distinguished
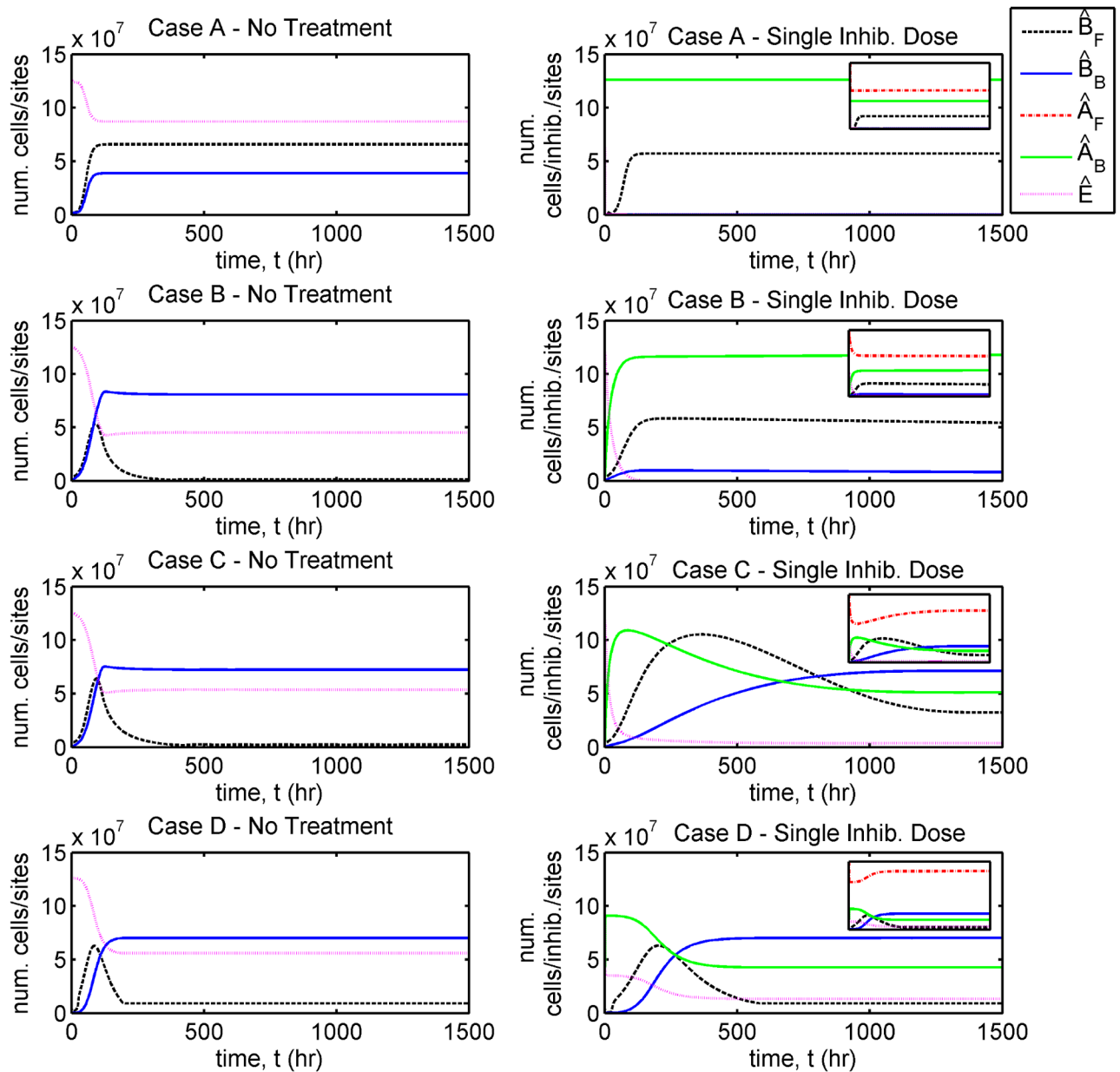
Fig 6. Comparison of dependent variables with and without a single dose of inhibitor. The total number of cells ($\hat{B}_F(t) = VB_F(t)$, $\hat{B}_B(t) = A_r B_B(t)$), inhibitors ($\hat{A}_F(t) = VA_F(t)$, $\hat{A}_B(t) = A_r A_B(t)$) and binding sites ($\hat{E}(t) = A_r E(t)$) are plotted in each case. Simulations extend beyond the time span of the experiments, to 1500 hours = 62.5 days. The insets in the right-hand column show the same plots as in the larger panels, but with the *y*-axis spanning $[0, 3 \times 10^8]$. Cases A and B: the number of bound bacteria are reduced as a result of treatment; Case C: treatment results in an increase in the number of free bacteria; Case D: treatment increases the time taken to reach a roughly equivalent steady-state to that without treatment. Eqs 1–8 were solved using ode15s. See Tables 1 and 2 for parameter values.

from the latter by the use of the word 'constant'. We also distinguish between the intrinsic growth rate, e.g., r_F, and the rate of logistic growth, e.g., $r_F B_F (1 - B_F/K_F)$.

The time-dependent results are summarised in Table 4. Treatments are most effective in Case A, some of them eliminating the bacterial burden completely. Most treatment scenarios are also effective in Case B. Surprisingly, treatment with inhibitors can actually increase the bacterial burden in Case C, although some treatments are still effective, while in Case D
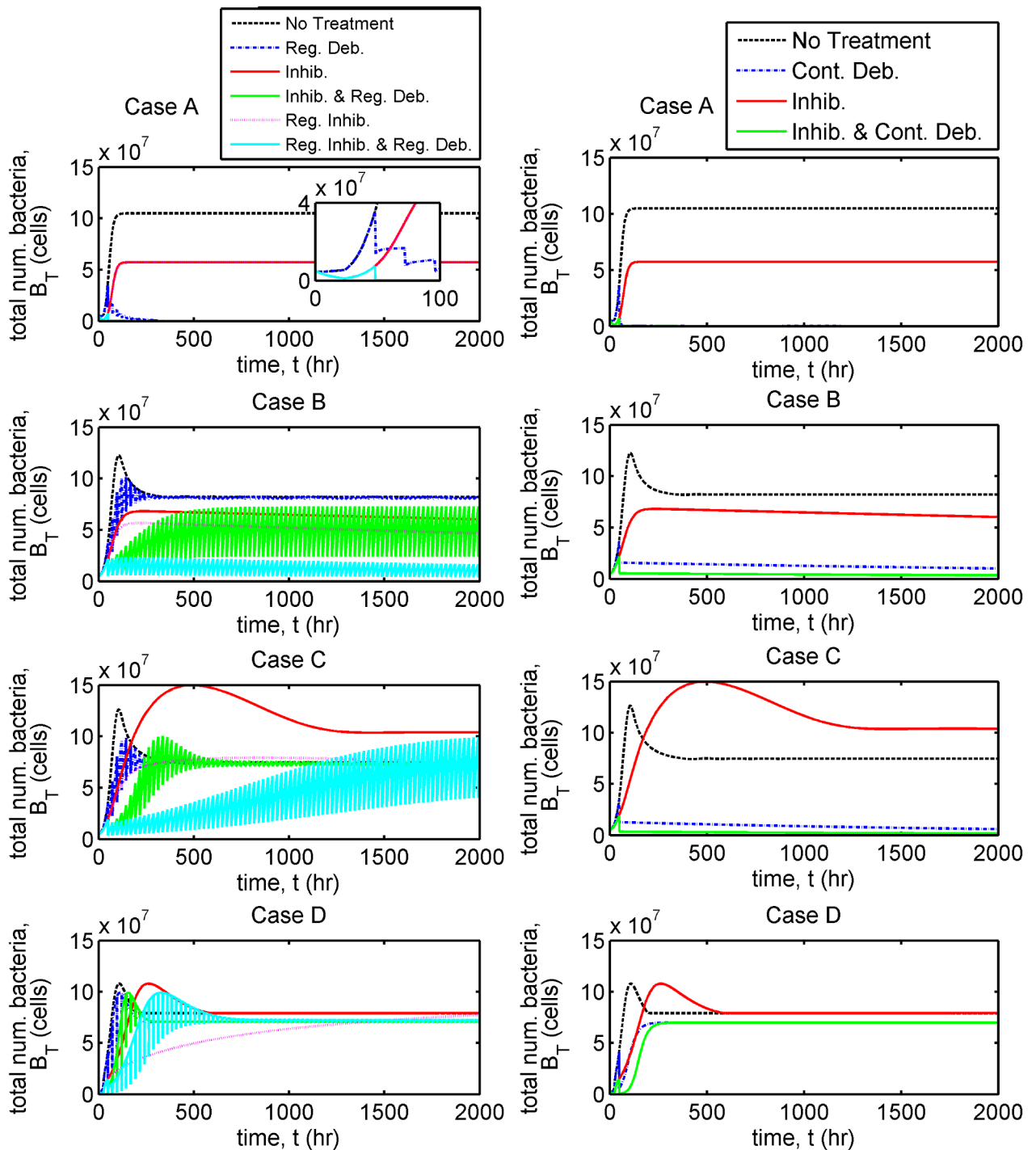
Fig 7. Comparison of bacterial population dynamics under a variety of treatment regimes. The total number of bacteria, $B_T(t)$ ($= VB_F(t) + A_r B_B(t)$), is plotted in each case. Simulations extend beyond the time span of the experiments, to 2000 hours ≈ 83 days. The untreated and single inhibitor dose ('Inhib.') scenarios are identical to those in Fig 5. See Treatment scenarios for a description of each treatment strategy. Case A: all treatments except single and regular inhibitor ('Reg. Inhib.') doses eradicate the bacterial population (such that $B_T(t) < 1$); Case B: regular inhibitor doses with regular debridement ('Reg. Inhib. and Reg. Deb.') and a single inhibitor dose with continuous debridement ('Inhib. and Cont. Deb.') are most effective, reducing the bacterial population size by an order of magnitude or more; Case C: only treatments involving continuous debridement ('Cont. Deb.' and 'Inhib. and Cont. Deb.') are effective, reducing the bacterial population size by an order of magnitude or more; Case D: no treatment strategy is effective. Eqs 1–8 were solved using ode15s. See Tables 1 and 2 for parameter values.

https://doi.org/10.1371/journal.pcbi.1006071.g007

Table 4. Summary of results.

Treatment scenario	Case A	Case B	Case C	Case D
Single inhibitor dose	(✓)	(✓)	✗	—
Regular inhibitor doses	(✓)	(✓)	✗/—/(✓)	—
Regular debridement	✓	—/(✓)	—/(✓)	—
Single inhibitor dose with regular debridement	✓	✗/—/(✓)	—/(✓)	—
Regular inhibitor doses with regular debridement	✓	(✓)/✓	✗/—/✓	—
Continuous debridement	✓	(✓)/✓	—/(✓)/✓	—
Single inhibitor dose with continuous debridement	✓	(✓)/✓	—/✓	—

'✓' (dark green): treatment is highly effective, reducing the bacterial burden by at least two orders of magnitude and in some cases eliminating it completely; '(✓)' (light green): treatment is effective, reducing the bacterial burden by no more than two orders of magnitude; '—' (yellow): treatment has little effect; '✗' (red) treatment increases the bacterial burden. Multiple symbols are used in those cases and treatment scenarios where there is variation between parameter sets; in this situation the cell colour corresponds to the least effective treatment. (Colour online.)

https://doi.org/10.1371/journal.pcbi.1006071.t004

all treatments are ineffective, the bacterial burden settling to its untreated steady-state in all scenarios.

When effective, treatment with inhibitors may reduce the total bacterial burden in two ways. Firstly, inhibitors may reduce the number of bound bacteria through competition for binding sites. The second way, which may follow as a consequence of the first, is by reducing the rate of production of daughter cells by bound bacteria.

We note that the maximum proportion of bound daughter cells to enter the bound compartment, η_{max}, ranges between $O(10^{-10})$ and $O(10^{-2})$, across the 12 parameter sets considered (see Table 1, and Table A in S2 Supporting Information). Therefore, the majority of bound daughter cells enter the exudate in all cases (though, once there, they will not continue to divide if the free carrying capacity is exceeded). This insight is not intuitively obvious, demonstrating the benefit of mathematical modelling.

Case A. Case A includes parameter sets 1 and 2 (see S2 Supporting Information), where the results from Set 2 are presented in the main text.

In Case A, inhibitors are predicted to bind rapidly to the surface, achieving quasi-steady-state in 15–30 mins in the single dose scenario (see Fig 6, and Fig F in S2 Supporting Information). This reduces the number of bound bacteria, compared with the untreated scenario, and, as a consequence, reduces the contribution of daughter cells to the exudate from the bound compartment (compare Figs G and I in S2 Supporting Information). In Set 2, the treatment-induced reduction in $B_T(t)$ is due largely to the drop in the number of bound bacteria as a result of replacement by inhibitors (the drop in $B_F(t)$ being small), while in Set 1 the latter effect is the more significant, the reduced flux of bound daughter cells into the free compartment resulting in a significant reduction in the number of free bacteria.

Surprisingly, the total number of free bacteria, $\hat{B}_F(t)$, is predicted to exceed its carrying capacity, VK_F, at steady-state, in the untreated scenario, in both Sets 1 and 2 (and thus the logistic growth term becomes a death term). This is valid since, as noted in Model formulation, the carrying capacities in this model represent the maximum number of bacteria that can be supported with nutrients in each compartment, rather than the maximum number that can fit into each compartment. Examination of the sizes of the terms in Eq 1 (see Fig G in S2 Supporting Information) reveals that this is due to the contribution of daughter cells from the bound compartment, the bacterial binding and unbinding rates essentially balancing each other.

Regular inhibitor dosing results in a total bacterial population size almost identical to that in the single inhibitor dose case. Each of the other treatment regimes examined are predicted to be successful in eliminating the bacterial population (such that $B_T(t) < 1$) given sufficient time—regular debridement takes the longest at 200 hr (Set 1) or 1700 hr (Set 2), while continuous debridement takes 70 hr (Set 1) or 140 hr (Set 2) and treatments combining inhibitor with regular or continuous debridement are much more rapid, elimination of bacteria occurring upon the initial debridement event at 48 hr (see Fig 7, and Figs M and N in S2 Supporting Information). Regular and continuous debridement are effective in eliminating bacteria in both Sets 1 and 2, even when inhibitors are not used, since the rate constant of bacterial unbinding is high (see Table 1, and Table A in S2 Supporting Information).

Case B. Case B includes parameter sets 3–7 (see S2 Supporting Information), where the results from Set 3 are presented in the main text.

The inhibitor binding rate constants in Case B are 4–5 orders of magnitude lower than those in Case A (see Table 1, and Table A in S2 Supporting Information) and consequently inhibitors take longer to reach quasi-steady-state—on the order of 100–200 hr compared with 15–30 mins for Case A. Having reached quasi-steady-state, inhibitors continue to bind at a lower rate than during the initial rapid phase (see Fig 6, and Fig F in S2 Supporting Information, and see Cases C and D below for comparison).

Treatment with inhibitors results in a significant reduction in the steady-state population size of bound bacteria (see Fig 6, and Fig F in S2 Supporting Information). However, surprisingly, it may either increase (Sets 3, 4 and 6) or decrease (Sets 5 and 7) the number of free bacteria, depending upon the effect of treatment upon the logistic growth of bound bacteria. Due to the quadratic dependence of the logistic growth rate of bound bacteria upon their density, a drop in the density of bound bacteria may either increase of decrease the rate of logistic growth and hence the flux of bound daughter cells into the free compartment. This is determined by the densities between which the bound compartment shifts and the bound carrying capacity (see Fig 8). Despite this, a single inhibitor dose is effective in reducing the total bacterial population size in all parameter sets, since the loss in bound bacteria is greater than the gain in free bacteria.

Regular debridement alone is predicted to be ineffective since there are a significant number of bound bacteria at the untreated steady-state and the rate constants of bacterial unbinding are much lower than in Case A (see Table 1, and Table A in S2 Supporting Information); however, continuous debridement is effective since free bacteria are eliminated while bound bacteria unbind gradually from the surface and are cleared (see Fig 7, and Figs M and N in S2 Supporting Information). Combining continuous debridement with inhibitors improves efficacy, compared with continuous debridement alone, as would be expected (see Fig N in S2 Supporting Information). Of those treatments which involve regular debridement, that which includes regular inhibitor doses is most effective, the inhibitors serving to displace the bound bacteria and debridement to remove free bacteria.

Case C. Case C includes parameter sets 8–11 (see S2 Supporting Information), where the results from Set 8 are presented in the main text.

In the untreated scenario, $B_T(t)$ evolves in a qualitatively similar way to Cases B and D; however, we have the surprising result that application of a single inhibitor dose leads to an increase in $B_T(t)$ at steady-state.

This last result may be explained as follows. The number of bound bacteria exceeds that of free bacteria in the untreated scenario for all parameter sets in Case C (see Fig 6, and Fig E in S2 Supporting Information). Application of a single inhibitor dose results in a slight reduction in the number of bound bacteria in Sets 8, 9 and 11 and a slight increase in Set 10, while the number of free bacteria increases by an order of magnitude or more in all sets (Fig F in
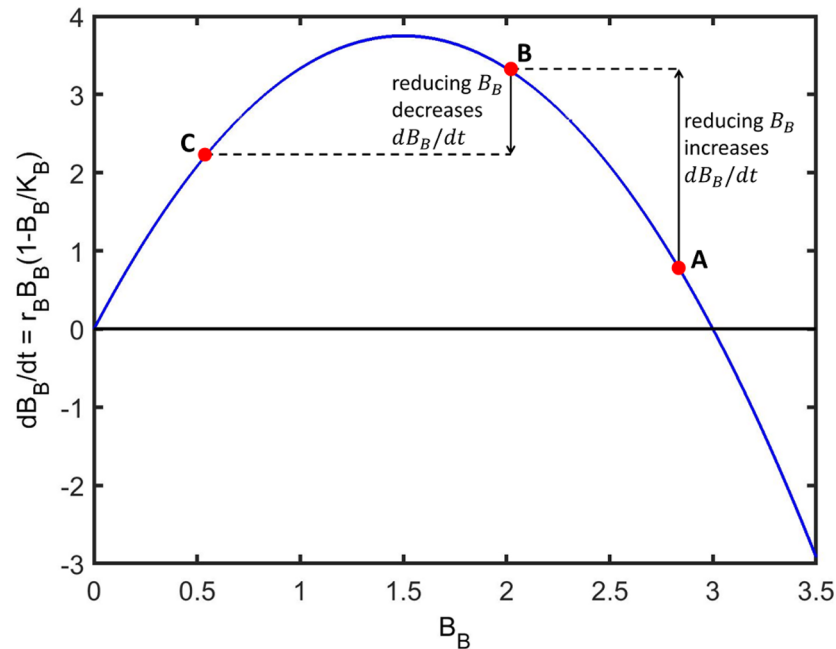
Fig 8. The effect of a drop in bound bacterial density upon their logistic growth rate. Treatment with inhibitor usually results in a drop in the density of bound bacteria, $B_B(t)$. The effect of this reduction in $B_B(t)$ upon the logistic growth rate, $dB_B/dt = r_B B_B(1 - B_B/K_B)$, depends upon the untreated value of $B_B(t)$, the value to which it is reduced and the carrying capacity, K_B. In this example, a reduction in $B_B(t)$ from A to B results in an increase in the logistic growth rate, while a reduction from B to C results in a decrease in the logistic growth rate. Parameter choices are for demonstration purposes only.

S2 Supporting Information). Inhibitors bind more rapidly to the host cells than bacteria, with $A_B(t)$ achieving its maximum value between 40–120 hr. However, whereas $A_B(t)$ is a monotone increasing function in Cases A and B, in Case C it slowly decreases, subsequent to the initial, more rapid, binding phase. Inhibitors outcompete bacteria for binding sites initially because they greatly outnumber them; however, as the number of free bacteria increases, bacteria begin to replace inhibitors. This is because, while the binding rate constants of bacteria and inhibitors are of the same order of magnitude, inhibitors have much higher unbinding rate constants, such that their association constant is much smaller (see Table 1, and Table A in S2 Supporting Information). The difference between association constants is less significant in Set 11, hence the effect is less pronounced in this case (see Fig F in S2 Supporting Information).

Bacteria are predicted to populate the bound compartment mainly through binding (as opposed to logistic growth) in both the untreated and single inhibitor dose scenarios, but the binding rate is lower in the treated scenario, since inhibitors reduce the number of free binding sites (see Figs H and J in S2 Supporting Information). Consequently, it takes bound bacteria longer to reach their steady-state value, during which time the logistic growth of bound bacteria is maintained at a higher level (the population size being kept well below carrying capacity at which logistic growth would go to zero), the majority of daughter cells entering the free compartment, pushing the population size of free bacteria well above untreated levels. As bound bacteria approach their carrying capacity their logistic growth rate diminishes, reducing the supply of bacteria to the free compartment and the system settles to steady-state.

Regular debridement and/or inhibitor doses are ineffective in significantly reducing the bacterial population size, except in Set 11, where regular inhibitor doses with regular

debridement reduced the population size by three orders of magnitude (Fig 7, and Fig M in S2 Supporting Information). Continuous debridement with and without inhibitor is effective in all cases except Set 10 where $B_T(t)$ tends to untreated levels at steady-state (Fig 7, and Fig N in S2 Supporting Information). Treatments involving continuous debridement reduce $B_T(t)$ by an order of magnitude in Sets 8 and 9 and to $O(100)$ or below in Set 11. No treatment is successful in completely eliminating the bacteria burden.

Case D. Case D consists of parameter set 12, which is presented in the main text.

Application of a single inhibitor dose slows the dynamics of the system, but results in essentially the same numbers of free and bound bacteria at steady-state (see Fig 6, and Figs E and F in S2 Supporting Information). Inhibitors bind rapidly initially, reaching quasi-steady-state in a couple of hours. This is followed by a more gradual period of unbinding as bacteria outcompete inhibitors for binding sites (see Fig 6, and Fig F in S2 Supporting Information). Inhibitors slow the dynamics by reducing the rate at which bacteria bind to the surface and by reducing the proportion of bound daughter cells which can remain bound to the surface.

Sensitivity analysis suggests that all treatments would be improved if K_B could be reduced in some way (see Fig O–V in S2 Supporting Information).

Inhibitor sensitivity analysis. We have seen above that treatment is always effective in Case A, is sometimes effective in Cases B and C and is never effective in Case D. The question then arises: can we modify the treatment strategies in such a way as to make at least some of them effective in all cases? In this section we explore two ways in which this might be achieved. Firstly, we investigate how treatment efficacy varies with changes in the binding and unbinding rate constants of inhibitors (α_A and β_A); and, secondly, we examine the effect of increasing the number of inhibitors used in each inhibitor dose (see Sensitivity analyses for details). Since we are varying parameters which relate only to the inhibitors, we consider only those five treatment scenarios that involve dosing with inhibitor.

The panels in Fig 9 and Figs W–AF in S2 Supporting Information show $\log_{10}(B_T(672))$ at each point in $(\log_{10}(\alpha_A), \log_{10}(\beta_A))$ parameter space (where 672 hr = 4 weeks). Red curves mark the contours along which $B_T(672) = 1$ and thus demarcate the boundary between the region of parameter space to the left of the curve, where $B_T(672) > 1$ and treatment has failed to eradicate the bacterial population, and the region to the right of the curve, where $B_T(672) < 1$ and treatment has successfully eliminated the bacterial population. In this section, we consider treatment to be effective only if it eliminates the bacterial burden, such that $B_T(672) < 1$.

Examination of Figs W–Z in S2 Supporting Information reveals that neither single nor regular inhibitor doses are predicted to be capable of eliminating the bacterial population for any of the 12 parameter sets considered. In contrast, the remaining three treatments (a single inhibitor dose with regular debridement, regular inhibitor doses with regular debridement and a single inhibitor dose with continuous debridement) are all predicted to be capable of eradicating the bacterial population, provided that the inhibitor binding rate constant is high enough and the unbinding rate constant is low enough. Therefore, in what follows, we focus upon these three treatment scenarios (Fig 9, and Figs AA–AF in S2 Supporting Information).

Treatment is predicted to be successful throughout the region of parameter space considered for all three treatment scenarios in Set 1 and for the single inhibitor dose with continuous debridement scenario in Set 2 (see Fig 9, and Figs AA–AF in S2 Supporting Information). Indeed, continuous debridement alone is successful in both Sets 1 and 2 as is regular debridement alone in Set 1 (see Fig 7, and Figs M and N in S2 Supporting Information). Each treatment strategy is more effective, that is bacteria are eliminated in a larger region of (α_A, β_A) parameter space, when more inhibitors are used per dose. On average, across the 12 parameter sets, a single inhibitor dose with continuous debridement is predicted to be the most effective strategy, followed by regular inhibitor doses with regular debridement and then single inhibitor dose with
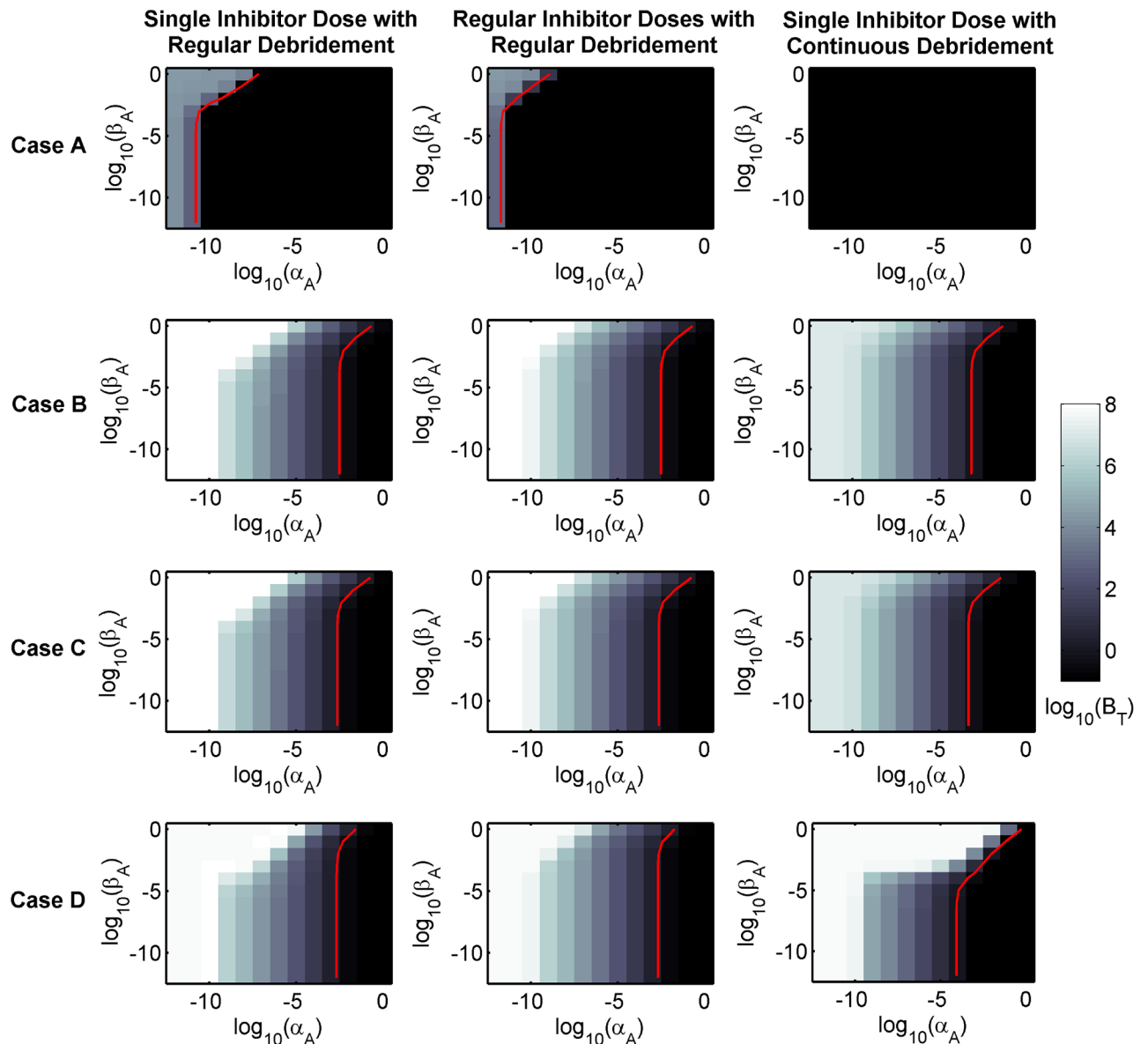
Fig 9. Sensitivity analysis to determine the effect of varying inhibitor adhesion kinetics upon treatment efficacy. For each panel, α_A and $\beta_A = 10^{-12}$, $10^{-11}, \ldots, 10^{-1}$ and 1, where a $\log_{10}$ scale is used on both axes. The value of $\log_{10}(B_T(672))$ is plotted at each point in parameter space, where $B_T(672)$ $(= VB_F(672) + A_r B_B(672))$ is the total number of bacteria after 4 weeks (672 hr). The colour scheme is calibrated to maximise clarity, such that values of $\log_{10}(B_T(672)) \leq -1$ appear in black. The red curve (colour online) traces the contour along which $B_T(672) = 1$, such that $B_T(672) > 1$ to the left and $B_T(672) < 1$ to the right of this curve. Treatment efficacy improves with increasing α_A and decreasing β_A. On average, treatment with a single inhibitor dose with continuous debridement is the most effective treatment, followed by regular inhibitor doses with regular debridement; a single inhibitor dose with regular debridement being the least effective of the three. Eqs 1–8 were solved using ode15s. $A_{F_{init}} = 6.12 \times 10^7$ inhibitors cm^{-3} (the standard value). See Tables 1 and 2 for the remaining parameter values.

https://doi.org/10.1371/journal.pcbi.1006071.g009

regular debridement (see Fig 9, and Figs AA–AF in S2 Supporting Information). Treatment efficacy shows a greater sensitivity to α_A than to β_A in the ranges considered for these parameters, such that even for values as large as $\beta_A = 1$ hr^{-1}, a value of α_A can be found such that treatment eliminates the bacterial population for all treatment strategies, doses and parameter sets.

Fig 10 shows the evolution in the total number of bacteria, $B_T(t)$, for the full range of treatment strategies in Cases A–D, where $\alpha_A = 10^{-2}$ hr^{-1} sites^{-1} and $\beta_A = 10^{-2}$ hr^{-1}. These values
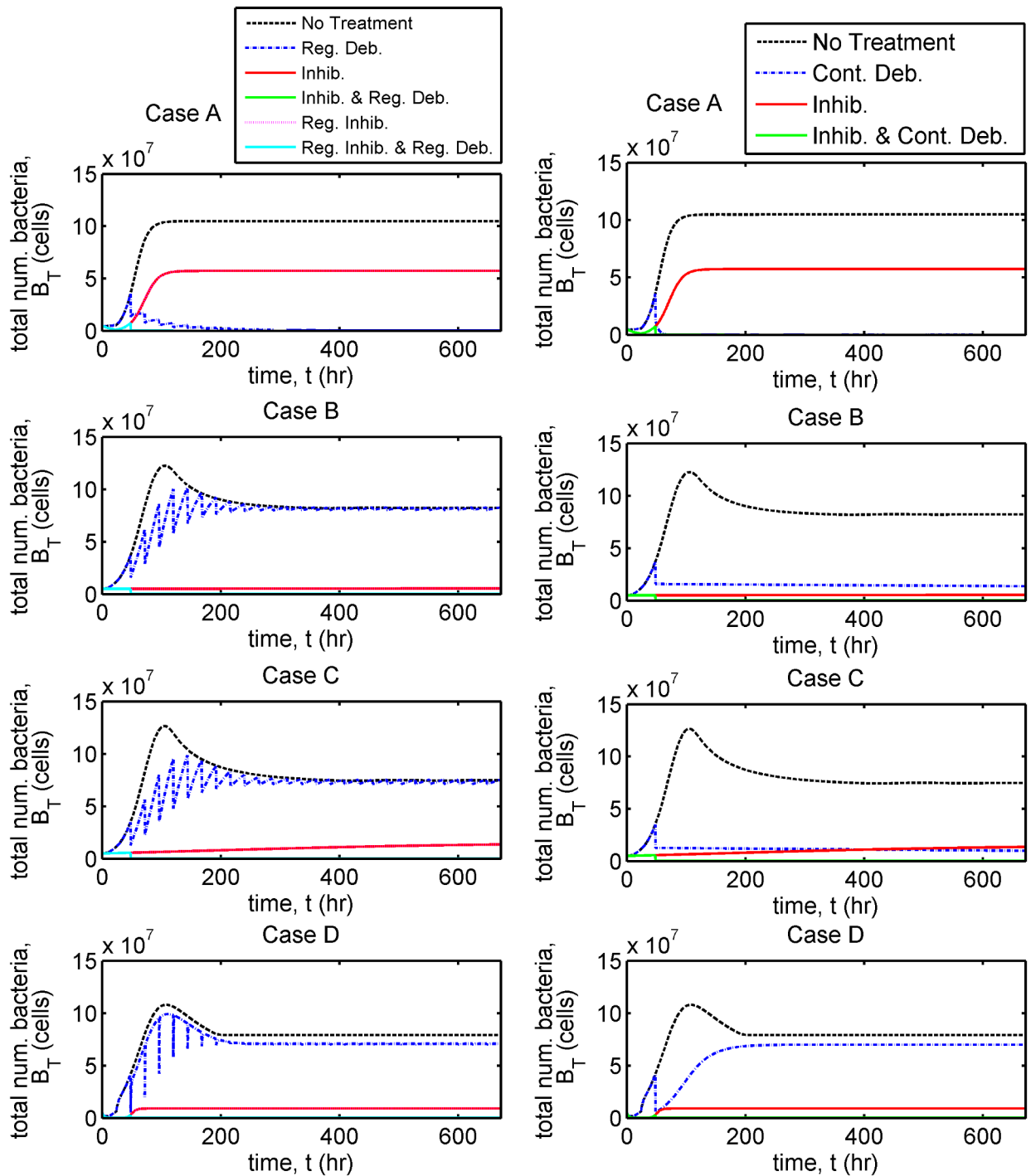
Fig 10. Comparison of bacterial population dynamics under a variety of treatment regimes with modified inhibitors. The total number of bacteria, $B_T(t)$ (= $VB_F(t) + A_rB_B(t)$), is plotted in each case. Simulations extend beyond the time span of the experiments, to 672 hours = 28 days. Bacteria are eliminated ($B_T(t) < 1$) by t = 672 hr for all treatment strategies combining inhibitor with regular or continuous debridement in all cases. In Case D, $B_T(672) > 1$; however, it descends below 1 at an earlier time point so bacteria may be considered to have been eliminated by t = 672 hr. Eqs 1–8 were solved using `ode15s`. Parameter values: $\alpha_A = 10^{-2}$ hr^{-1} sites^{-1} and $\beta_A = 10^{-2}$ hr^{-1}. See Tables 1 and 2 for the remaining parameter values.

https://doi.org/10.1371/journal.pcbi.1006071.g010

are chosen, based upon the sensitivity analysis above, such that all those treatment strategies which combine inhibitor with regular or continuous debridement are effective in eliminating the bacterial population, that is $B_T(672) < 1$. The only exception is for the single inhibitor dose with continuous debridement treatment in Case D, where $B_T(672) \approx 1.07$; however, $B_T(t) < 1$ for $t \in (48, 665)$, so treatment can be considered to have eliminated the bacterial population in this case also. Therefore, our models make the encouraging prediction that, in theory, treatment could be rendered successful in all cases.

Discussion

As bacteria gain increasing resistance to antibiotics it is vital that we develop alternative treatment strategies. Anti-virulence treatments—specifically MAM7-coupled beads, which operate by competitively inhibiting the binding of bacteria to host cells—present a promising complement or alternative to antibiotics. Opinion as to the likely efficacy of such treatments is mixed, with some suggesting that their utility may be limited to preventing the initiation of a bacterial infection (prophylaxis) as opposed to treating a pre-existing infection (therapy) [6, 10, 47, 48]. In this paper we have used mathematical models to help us interpret the results of an experimental model, involving the inhibitor treatment of a burn wound infected by *P. aeruginosa* in the rat (see Experimental set-up). Our models allow us to predict the conditions under which treatment with inhibitors will be effective and to explore ways in which inhibitor dosing could be augmented to improve efficacy.

Mathematical models were fitted to experimental data using a combination of MCMC and frequentist techniques (Parameter fitting). A number of close fits were obtained (12 parameter sets are explored here) and classified into four qualitatively different cases (A–D).

Given the significant qualitative, and not merely quantitative, differences in predicted treatment outcomes between Cases A–D, this work highlights the importance of considering a range of viable parameter sets. Had a single parameter set been chosen, our conclusions would have differed markedly from those in this more comprehensive study. It may be that different parameters sets could reflect inter-patient variability, as well as different bacterial species. Indeed, a variety of Gram negative and Gram positive bacteria have been found to infect burn wounds (see, for example, [15–17, 19]).

Eight treatment scenarios were considered for each of Cases A–D (see Treatment scenarios for details). The untreated and single inhibitor dose scenarios were considered in the experimental model, while the rest are theoretical treatments that remain to be tested experimentally. Continuous debridement, with clearance rates on the order of magnitude of those used in simulations, is probably not practically achievable; though it might be possible to maintain a high level of clearance using negative pressure wound therapy (see Introduction). In any case, these simulations allow us to determine the theoretical best-case scenario where debridement is applied.

Simulations for the 8 treatment scenarios in Cases A–D reveal a range of outcomes and provide insight into the bacterial population dynamics (Case A–Case D). Before considering each case in turn, a few general observations can be made. Firstly, while the ratio between the number of bacteria at carrying capacity in the free and bound compartments, VK_F and A_rK_B respectively, varies between parameter sets, the intrinsic growth rate in the bound compartment, r_B, is consistently greater than that of the free compartment, r_F (see Table 1 and Table A in S2 Supporting Information). This suggests that the bound compartment is more favourable to the growth of bacteria than the free compartment, agreeing nicely with Huebinger *et al.*'s [23] speculative explanation for the efficacy of inhibitor treatment. This might be because bound bacteria have access to additional nutrients derived from the host cells, not available to free bacteria.

Our model predicts that in order for inhibitor treatment to be effective, inhibitors must bind rapidly and numerously. If they do not, then treatment may actually worsen a bacterial infection. If inhibitors bind in sufficient quantities to the host cells, then the number of bacteria in the bound compartment and hence their rate of logistic growth will remain small, reducing the flux of bound daughter cells into the free compartment. However, if inhibitors bind in lower numbers, then while the number of bound bacteria at steady-state may be reduced, their logistic growth rate increases (see Fig 8) as does the flux of bound daughter cells into the free compartment, with the result that inhibitor treatment increases the total number of bacteria at steady-state above its untreated value.

If debridement is applied too early, as in Set 7, it may reduce treatment efficacy as inhibitors will have had insufficient time to bind before those in the free compartment are removed. If inhibitor binding rates could be determined experimentally then this would allow us to determine the optimum timing of debridement in relation to inhibitor dosing.

All treatments are effective in significantly reducing the bacterial population size in Case A. In Case B, all treatments except regular debridement and a single inhibitor dose with regular debridement are consistently effective. Counterintuitively, a single inhibitor dose increases the bacterial burden in Case C, with treatments involving continuous debridement being the most effective. Lastly, in Case D, all of the treatment strategies result in a steady-state bacterial population size similar to that without treatment.

The differences in behaviour between Cases A–D may be explained, to some extent, by the differences in the bacteria and inhibitor association constants and the ratio of these constants (see Table 1, and Table A in S2 Supporting Information). The bacteria association constant is lower in Case A than in Cases B–D, while the inhibitor association constant and the ratio of these constants are lowest in Case A, highest in Cases C–D and take intermediate values in Case B. Treatments are more effective where the inhibitor association constant is higher and the bacterial association constant is lower, and hence where the ratio of association constants is lower. The qualitative difference between Cases C and D is less significant than between the other cases, thus it is not surprising that the order of magnitude of their association constants and their ratio are not distinct.

Given the correlation between bacteria and inhibitor association constants and treatment efficacy, a natural way to seek to improve treatment would be to decrease the bacterial association constant or to increase the inhibitor association constant, shifting the system behaviour towards that in Case A. The bacterial association constant could be reduced by treating with a molecule that binds to and blocks bacterial adhesins used for binding to the host cells e.g. mannosides, which bind FimH [12]. In order for these molecules not to interfere with the inhibitor treatment they would need to either bind to an adhesin other than MAM7 or be applied to a wound before the inhibitor dose, giving the molecules time to bind to the bacteria. The inhibitor association constant could be increased by coupling more MAM7 molecules to each bead.

Sensitivity analysis of the inhibitor binding rate constant, unbinding rate constant and dose concentration predicts conditions under which treatments involving inhibitor would eliminate the bacterial burden within 28 days (Inhibitor sensitivity analysis, Fig 9, and Figs W–AF in S2 Supporting Information). Neither a single nor regular doses of inhibitor on their own were predicted to be capable of eliminating the bacterial population, though they may reduce it by several orders of magnitude. This is to be expected since, on its own, inhibitor can only prevent bacteria from entering the bound compartment, and is unable to remove bacteria from the free compartment. Encouragingly, when combined with regular or continuous debridement, inhibitor treatment is predicted to have the potential to eliminate the bacterial population. A single inhibitor dose with continuous debridement is predicted to be the most effective treatment, followed by regular inhibitor doses with regular debridement, with a single inhibitor

dose with regular debridement being the least effective of the three. Treatment is predicted to be more effective for higher binding rate constants, lower unbinding rate constants and higher concentration inhibitor doses, where treatment efficacy is more sensitive to the binding rate constant than to the unbinding rate constant.

In future work we will proceed on two fronts: experimental and theoretical. We will conduct further experiments to test our model predictions and to improve model parametrisation. Experiments like those described in Experimental set-up could be performed over a longer time-span and separate measurements made for the numbers of free and bound bacteria and inhibitors. This would enable us to refine the range of possible parameter sets. This would also be aided by more regular wound imaging than the current daily set-up. Further experiments to test the model predictions concerning the other treatment strategies suggested here would also be valuable. We will develop our mathematical modelling in at least two directions. Firstly, we will incorporate treatment with antibiotics, seeking to determine the optimum treatment regime when combined with inhibitor dosing and regular or continuous debridement. Secondly, we will consider a discrete-stochastic cellular automata model to capture some of the mechanisms in the system in more detail, including the spatial spread of infection, which has been shown experimentally to be limited upon treatment with inhibitor [23]. Our models could also be extended to incorporate quorum sensing and biofilm formation.

In conclusion, our mathematical models suggest that inhibitor treatment could be effective in eliminating or significantly reducing the bacterial burden in a burn wound when combined with regular or continuous debridement. Where inhibitor treatment is effective, it operates both by preventing bacteria from occupying the host cells (where growth rates are predicted to be higher) and, consequently, by reducing the flux of bound daughter cells into the exudate. Our model predicts that inhibitor treatments, in particular those involving regular or continuous debridement, could be effective when used both prophylactically and therapeutically. Our models further predict that treatment efficacy can be improved by optimising inhibitor design and dosing schedules.

Supporting information

S1 Supporting Information. Parameter fitting methods.
(PDF)

S2 Supporting Information. Data and results for all 12 parameter sets.
(PDF)

S3 Supporting Information. Steady-state analysis details.
(PDF)

S4 Supporting Information. Numerical solutions—Additional details.
(PDF)

Author Contributions

Conceptualization: Paul A. Roberts, Anne-Marie Krachler, Sara Jabbari.

Data curation: Paul A. Roberts.

Formal analysis: Paul A. Roberts.

Funding acquisition: Anne-Marie Krachler, Sara Jabbari.

Investigation: Paul A. Roberts, Ryan M. Huebinger, Emma Keen.

Methodology: Paul A. Roberts.

Project administration: Sara Jabbari.

Resources: Anne-Marie Krachler, Sara Jabbari.

Software: Paul A. Roberts.

Supervision: Anne-Marie Krachler, Sara Jabbari.

Validation: Paul A. Roberts.

Visualization: Paul A. Roberts.

Writing – original draft: Paul A. Roberts.

Writing – review & editing: Paul A. Roberts, Ryan M. Huebinger, Emma Keen, Anne-Marie Krachler, Sara Jabbari.

References

1. Brannon JR, Hadjifrangiskou M. The arsenal of pathogens and antivirulence therapeutic strategies for disarming them. Drug Des Devel Ther. 2016; 10:1795–1806. https://doi.org/10.2147/DDDT.S98939 PMID: 27313446

2. O'Neill, J, and The Review on Antimicrobial Resistance. Tackling drug-resistant infections globally: Final report and recommendations; 2016.

3. Nathan C, Cars O. Antibiotic Resistance—Problems, Progress, and Prospects. N Engl J Med. 2014; 371(19):1761–1763. https://doi.org/10.1056/NEJMp1408040 PMID: 25271470

4. Bush K, Courvalin P, Dantas G, Davies J, Eisenstein B, Huovinen P, et al. Tackling antibiotic resistance. Nat Rev Micro. 2011; 9(12):894–896. https://doi.org/10.1038/nrmicro2693

5. Teillant A, Gandra S, Barter D, Morgan DJ, Laxminarayan R. Potential burden of antibiotic resistance on surgery and cancer chemotherapy antibiotic prophylaxis in the USA: a literature review and modelling study. Lancet Infect Dis. 2015; 15(12):1429–1437. https://doi.org/10.1016/S1473-3099(15)00270-4 PMID: 26482597

6. Clatworthy AE, Pierson E, Hung DT. Targeting virulence: a new paradigm for antimicrobial therapy. Nat Chem Biol. 2007; 3(9):541–548. https://doi.org/10.1038/nchembio.2007.24 PMID: 17710100

7. Allen RC, Popat R, Diggle SP, Brown SP. Targeting virulence: can we make evolution-proof drugs? Nat Rev Micro. 2014; 12(4):300–308. https://doi.org/10.1038/nrmicro3232

8. Vale PF, Fenton A, Brown SP. Limiting Damage during Infection: Lessons from Infection Tolerance for Novel Therapeutics. PLoS Biol. 2014; 12(1):e1001769. https://doi.org/10.1371/journal.pbio.1001769 PMID: 24465177

9. Krachler AM, Ham H, Orth K. Turnabout is fair play. Virulence. 2012; 3(1):68–71. https://doi.org/10.4161/viru.3.1.18172 PMID: 22086133

10. Krachler AM, Orth K. Targeting the bacteria-host interface. Virulence. 2013; 4(4):284–294. https://doi.org/10.4161/viru.24606 PMID: 23799663

11. Rasko DA, Sperandio V. Anti-virulence strategies to combat bacteria-mediated disease. Nat Rev Drug Discov. 2010; 9(2):117–128. https://doi.org/10.1038/nrd3013 PMID: 20081869

12. Spaulding CN, Klein RD, Ruer S, Kau AL, Schreiber HL, Cusumano ZT, et al. Selective depletion of uropathogenic E. coli from the gut by a FimH antagonist. Nature. 2017; 546(7659):528–532. https://doi.org/10.1038/nature22972 PMID: 28614296

13. Krachler AM, Ham H, Orth K. Outer membrane adhesion factor multivalent adhesion molecule 7 initiates host cell binding during infection by Gram-negative pathogens. Proc Natl Acad Sci. 2011; 108 (28):11614–11619. https://doi.org/10.1073/pnas.1102360108 PMID: 21709226

14. Krachler AM, Orth K. Functional Characterization of the Interaction between Bacterial Adhesin Multivalent Adhesion Molecule 7 (MAM7) Protein and Its Host Cell Ligands. J Biol Chem. 2011; 286 (45):38939–38947. https://doi.org/10.1074/jbc.M111.291377 PMID: 21937438

15. Church D, Elsayed S, Reid O, Winston B, Lindsay R. Burn Wound Infections. Clin Microbiol Rev. 2006; 19(2):403–434. https://doi.org/10.1128/CMR.19.2.403-434.2006 PMID: 16614255

16. Azzopardi EA, Azzopardi E, Camilleri L, Villapalos J, Boyce DE, Dziewulski P, et al. Gram Negative Wound Infection in Hospitalised Adult Burn Patients-Systematic Review and Metanalysis-. PLoS ONE. 2014; 9(4):e95042. https://doi.org/10.1371/journal.pone.0095042 PMID: 24751699

17. Öncül O, Öksüz S, Acar A, Ülkür E, Turhan V, Uygur F, et al. Nosocomial infection characteristics in a burn intensive care unit: Analysis of an eleven-year active surveillance. Burns. 2014; 40(5):835–841. https://doi.org/10.1016/j.burns.2013.11.003 PMID: 24296064

18. Pruitt BA Jr, McManus AT, Kim SH, Goodwin CW. Burn Wound Infections: Current Status. World J Surg. 1998; 22(2):135–145. https://doi.org/10.1007/s002689900361 PMID: 9451928

19. Weber JM, Sheridan RL, Pasternack MS, Tompkins RG. Nosocomial infections in pediatric patients with burns. Am J Infect Control. 1997; 25(3):195–201. https://doi.org/10.1016/S0196-6553(97)90004-3 PMID: 9202814

20. Mouës CM, Vos MC, Van Den Bemd GJCM, Stijnen T, Hovius SER. Bacterial load in relation to vacuum-assisted closure wound therapy: A prospective randomized trial. Wound Rep Reg. 2004; 12 (1):11–17. https://doi.org/10.1111/j.1067-1927.2004.12105.x

21. Mendonca DA, Papini R, Price PE. Negative-pressure wound therapy: a snapshot of the evidence. Int Wound J. 2006; 3(4):261–271. https://doi.org/10.1111/j.1742-481X.2006.00266.x PMID: 17199762

22. Vikatmaa P, Juutilainen V, Kuukasjärvi P, Malmivaara A. Negative Pressure Wound Therapy: a Systematic Review on Effectiveness and Safety. Eur J Vasc Endovasc. 2008; 36(4):438–448. https://doi.org/10.1016/j.ejvs.2008.06.010

23. Huebinger RM, Stones DH, de Souza Santos M, Carlson DL, Song J, Vaz DP, et al. Targeting bacterial adherence inhibits multidrug-resistant Pseudomonas aeruginosa infection following burn injury. Sci Rep. 2016; 6(39341). https://doi.org/10.1038/srep39341 PMID: 27996032

24. Krachler AM, Mende K, Murray C, Orth K. In vitro characterization of multivalent adhesion molecule 7-based inhibition of multidrug-resistant bacteria isolated from wounded military personnel. Virulence. 2012; 3(4):389–399. https://doi.org/10.4161/viru.20816 PMID: 22722243

25. Hawley CA, Watson CA, Orth K, Krachler AM. A MAM7 Peptide-Based Inhibitor of Staphylococcus aureus Adhesion Does Not Interfere with In Vitro Host Cell Function. PLoS ONE. 2013; 8(11):e81216. https://doi.org/10.1371/journal.pone.0081216 PMID: 24265842

26. Anguige K, King JR, Ward JP, Williams P. Mathematical modelling of therapies targeted at bacterial quorum sensing. Math Biosci. 2004; 192(1):39–83. https://doi.org/10.1016/j.mbs.2004.06.008 PMID: 15494175

27. Anguige K, King JR, Ward JP. Modelling antibiotic- and anti-quorum sensing treatment of a spatially-structured Pseudomonas aeruginosa population. J Math Biol. 2005; 51(5):557–594. https://doi.org/10.1007/s00285-005-0316-8 PMID: 16012802

28. Anguige K, King JR, Ward JP. A multi-phase mathematical model of quorum sensing in a maturing Pseudomonas aeruginosa biofilm. Math Biosci. 2006; 203(2):240–276. https://doi.org/10.1016/j.mbs.2006.05.009 PMID: 16962618

29. Fagerlind MG, Nilsson P, Harlén M, Karlsson S, Rice SA, Kjelleberg S. Modeling the effect of acylated homoserine lactone antagonists in Pseudomonas aeruginosa. Biosystems. 2005; 80(2):201–213. https://doi.org/10.1016/j.biosystems.2004.11.008 PMID: 15823419

30. Koerber AJ, King JR, Ward JP, Williams P, Croft JM, Sockett RE. A mathematical model of partial-thickness burn-wound infection by Pseudomonas aeruginosa: Quorum sensing and the build-up to invasion. Bull Math Biol. 2002; 64(2):239–259. https://doi.org/10.1006/bulm.2001.0272 PMID: 11926116

31. Jabbari S, King JR, Williams P. A mathematical investigation of the effects of inhibitor therapy on three putative phosphorylation cascades governing the two-component system of the agr operon. Math Biosci. 2010; 225(2):115–131. https://doi.org/10.1016/j.mbs.2010.03.001 PMID: 20214910

32. Jabbari S, King JR, Williams P. Cross-Strain Quorum Sensing Inhibition by Staphylococcus aureus. Part 1: A Spatially Homogeneous Model. Bull Math Biol. 2012; 74(6):1292–1325.

33. Jabbari S, King JR, Williams P. Cross-Strain Quorum Sensing Inhibition by Staphylococcus Aureus. Part 2: A Spatially Inhomogeneous Model. Bull Math Biol. 2012; 74(6):1326–1353. https://doi.org/10.1007/s11538-011-9702-0 PMID: 22108738

34. Ternent L, Dyson RJ, Krachler AM, Jabbari S. Bacterial fitness shapes the population dynamics of antibiotic-resistant and -susceptible bacteria in a model of combined antibiotic and anti-virulence treatment. J Theor Biol. 2015; 372:1–11. https://doi.org/10.1016/j.jtbi.2015.02.011 PMID: 25701634

35. Hilhorst D, King JR, Röger M. Mathematical analysis of a model describing the invasion of bacteria in burn wounds. Nonlinear Anal Theory Methods Appl. 2007; 66(5):1118–1140. https://doi.org/10.1016/j.na.2006.01.009

36. Hilhorst D, King JR, Röger M. Travelling-wave analysis of a model describing tissue degradation by bacteria. Eur J Appl Math. 2007; 18(5):583–605. https://doi.org/10.1017/S0956792507007139

37. King JR, Koerber AJ, Croft JM, Ward JP, Williams P, Sockett RE. Modelling host tissue degradation by extracellular bacterial pathogens. Math Med Biol. 2003; 20(3):227–260. https://doi.org/10.1093/imammb/20.3.227 PMID: 14667046

38. Agyingi E, Maggelakis S, Ross D. The Effect of Bacteria on Epidermal Wound Healing. Math Model Nat Phenom. 2010; 5(3):28–39. https://doi.org/10.1051/mmnp/20105303

39. Orazov M, Sakiyama Y, Graves DB. Wound healing modeling: investigating ambient gas plasma treatment efficacy. Journal of Physics D: Applied Physics. 2012; 45(445201).

40. Freter R, Brickner H, Fekete J, Vickerman MM, Carey KE. Survival and Implantation of Escherichia coli in the Intestinal Tract. Infect Immun. 1983; 39(2):686–703. PMID: 6339389

41. van Gestel J, Nowak MA. Phenotypic Heterogeneity and the Evolution of Bacterial Life Cycles. PLoS Comput Biol. 2016; 12(2):e1004764. https://doi.org/10.1371/journal.pcbi.1004764 PMID: 26894881

42. Gefen O, Fridman O, Ronin I, Balaban NQ. Direct observation of single stationary-phase bacteria reveals a surprisingly long period of constant protein production activity. Proc Natl Acad Sci. 2014; 111 (1):556–561. https://doi.org/10.1073/pnas.1314114111 PMID: 24344288

43. Roostalu J, Jõers A, Luidalepp H, Kaldalu N, Tenson T. Cell division in Escherichia colicultures monitored at single cell resolution. BMC Microbiol. 2008; 8:68. https://doi.org/10.1186/1471-2180-8-68 PMID: 18430255

44. Cutting K. Wound exudate: composition and functions. Br J Community Nurs. 2003; 8:4–9. https://doi.org/10.12968/bjcn.2003.8.Sup3.11577

45. Gonzalez MR, Fleuchot B, Lauciello L, Jafari P, Applegate LA, Raffoul W, et al. Effect of Human Burn Wound Exudate on Pseudomonas aeruginosa Virulence. mSphere. 2016; 1(2):e00111–15. https://doi.org/10.1128/mSphere.00111-15 PMID: 27303724

46. Agay D, Andriollo-Sanchez M, Claeyssen R, Touvard L, Denis J, Roussel AM, et al. Interleukin-6, TNF-alpha and interleukin-1 beta levels in blood and tissue in severely burned rats. Eur Cytokine Netw. 2008; 19(1):1–7. PMID: 18299267

47. Cegelski L, Marshall GR, Eldridge GR, Hultgren SJ. The biology and future prospects of antivirulence therapies. Nat Rev Micro. 2008; 6(1):17–27. https://doi.org/10.1038/nrmicro1818

48. Zambelloni R, Marquez R, Roe AJ. Development of Antivirulence Compounds: A Biochemical Review. Chem Biol Drug Des. 2015; 85(1):43–55. https://doi.org/10.1111/cbdd.12430 PMID: 25521644